ADVANCES IN REMOTE SENSING OF RAINFALL AND SNOWFALL



Examining the role of unusually warm Indo-Pacific sea-surface temperatures in recent African droughts

Chris Funk^{1,2} | Laura Harrison² | Shraddhanand Shukla² | Catherine Pomposi² |
Gideon Galu^{2,3} | Diriba Korecha^{2,3} | Gregory Husak² | Tamuka Magadzire^{2,3} | Frank Davenport² |
Chris Hillbruner³ | Gary Eilerts⁴ | Benjamin Zaitchik⁵ | James Verdin⁴

Correspondence

Chris Funk, Climate Hazards Group 4716 Ellison Hall, University of California, Santa Barbara, CA 93106, California. Email: cfunk@usgs.gov

Funding information

NASA, NNX16AM02G. USGS, G14AC00042.

Southern Africa (SA) and eastern Africa (EA) experienced a sequence of severe droughts in December-February (SA DJF) 2015-2016, October-December (EA OND) 2016 and March-April-May 2017 (EA MAM). This sequence contributed to severe food insecurity. While climate variability in these regions is very complex, the goal of this study is to analyse the role played by unusually warm Indo-Pacific SSTs, where unusual is defined as a 1-in-6 year event. We use observed sea-surface temperatures (SST) and satellite-gauge rainfall observations, a 20-member ensemble of Community Atmospheric Model version 5.1 simulations (CAM5), and a 40-member ensemble of climate change simulations from the Community Earth Systems Model version 1 (CESM1) Large Ensemble Community Project (LENS) to explore climate conditions associated with warm events identified based on eastern and western Pacific SSTs. Our analysis suggests that strong El Niño's may be followed by warm western Pacific SST conditions, which can lead to conditions conducive to successive and potentially predictable droughts in SA DJF, EA OND and EA MAM. We show that different regions of warm SST are related to recent droughts—SA DJF: Niño 3.4; EA OND: western equatorial Pacific (WEP); and EA MAM: western North Pacific (WNP). For DJF and MAM, respectively, the CAM5 model driven with observed SST and the same model driven within a climate change experiment indicate that warmer El Niño's and WNP events produce more intense atmospheric responses, potentially associated with more severe droughts. OND climate seems to be strongly influenced by the Indian Ocean Dipole, which corresponds with some WEP events. Given global warming, we suggest that the extreme Niño 3.4 and west Pacific SST events responsible for 2015-2017 droughts are likely to reoccur, thus humanitarian agencies should prepare to predict and respond to multi-year drought and substantial food insecurity in SA and EA.

KEYWORDS

drought analysis, food security and climate change, general-circulation model experiments, health, observational data analysis, policy, remote sensing, seasonal prediction, surface-based observations

This is an open access article under the terms of the Creative Commons Attribution License, which permits use, distribution and reproduction in any medium, provided the original work is properly cited.

© 2018 The Authors. Quarterly Journal of the Royal Meteorological Society published by John Wiley & Sons Ltd on behalf of the Royal Meteorological Society.

Q J R Meteorol Soc. 2018;n/a. wileyonlinelibrary.com/journal/qj

¹U.S. Geological Survey, Center for Earth Resources Observation and Science, Sioux Falls, South Dakota

²UC Santa Barbara Climate Hazards Group, Santa Barbara, California

³Famine Early Warning Systems Network

⁴U.S. Agency for International Development,

Office of Food for Peace, Washington, D.C.

⁵Earth and Planetary Sciences, Johns Hopkins University, Baltimore, Maryland

1 | INTRODUCTION

In 2017, the world faced very high numbers of people suffering from severe food insecurity (FEWSNET, 2017b), unprecedented in the recent period. More than 81.3 million people (Table 1) required emergency food assistance. Levels of food insecurity have been building; in 2016, Famine Early Warning Systems Network (FEWS NET) estimated that 69.1 million people faced severe hunger, nutritional deficits, and elevated risks of stunting, wasting, and diseases like acute watery diarrhoea. While more than half of this food insecurity was related to conflict and political crises in Syria, Yemen, South Sudan and Nigeria, FEWS NET estimates that 23.5 million food-insecure people lived in areas suffering from drought impacts of the strong 2015/2016 El Niño (Ethiopia, southern Africa). This estimate rose to 29.1 million after back-to-back droughts struck East Africa during October-November-December (OND) of 2016 and March-April-May (MAM) of 2017. Motivated by these severe food crises, this study examines the role of unusually warm Indo-Pacific sea-surface temperatures (SST) in recent African droughts.

East African rainfall has very complex spatial and seasonal climate patterns (Liebmann et al., 2012; Nicholson, 2017). In general, the Greater Horn of Africa can be divided into three main regions: two unimodal regions that receive most of their rains in austral summer (central and southern Tanzania) and boreal summer (northern Ethiopia), and one region near the Equator that typically experiences bimodal rains in OND and MAM. Within this bimodal region, drought sensitivity tends to increase in the east, with eastern Kenya, Somalia, and southern Ethiopia exposed to frequent severe droughts. Since 2005, this region has experienced a high frequency of droughts in both OND and MAM with a tendency for droughts to persist across several seasons (Nicholson, 2016). The first studies to analyse recent increased drought occurrence during the long rains (MAM) (Verdin et al., 2005; Funk et al., 2008) focused on increased diabatic forcing and SST

TABLE 1 FEWS NET estimates of people facing crisis, emergency or famine levels of food insecurity for 2016–2017 (Frankenberger and Verduijn, 2011)

Region	2016	2017
Ethiopia	10.5 million	5.5 million
Rest of eastern Africa ^a	3.0 million	7.6 million
Southern Africa ^b	10.0 million	16 million
Total affected by ENSO	23.5 million	29.1 million
Global total requiring assistance	69.1 million	81.3 million

Note. These are the number of people FEWS NET and partner agencies estimated as urgently needing external food assistance. These populations are facing Crisis, Emergency, or Famine (IPC Phase 3 or greater) food insecurity outcomes.

within and over the Indian Ocean, positing that such warming was associated with a Matsuno–Gill-like response that produced subsidence over East Africa (EA). While the basic diabatic forcing–EA drought mechanism outlined in these studies is still pertinent, and the tendency for MAM drought has continued (Nicholson, 2017), recent work has emphasized the role of a preferential warming of the Indo-Pacific Warm Pool. Diagnostic analyses have suggested that this warming is related to a low-frequency intensification of the Walker Circulation (Williams and Funk, 2011), and Atmospheric Model Intercomparison Project (AMIP) simulations indicate that SST changes in the western and eastern Pacific have played a dominant role in producing these changes.

The observed EA MAM drying has been termed the "East African Climate Paradox" (Rowell et al., 2015) because of the discrepancy between the observed rainfall trends (Verdin et al., 2005; Funk et al., 2008) and climate change model predictions. Station data (Funk et al., 2015a; 2015b) and palaeoclimate data (Tierney et al., 2013; 2015) indicate declines, while models call for increases in EA rainfall. While research is ongoing, there are currently three major hypotheses being explored by three different research groups. These hypotheses are not mutually exclusive. One hypothesis, advanced by Tierney et al. (2015), is that the "paradox" may be largely due to the models' inability to simulate the long rains well. The EA long rains in the models are much lower than the OND short rains, too low, and thus a simulated El Niño-like climate shift increases annual totals through overestimated positive OND impacts. Another hypothesis has been that the primary driver of EA drying has been Pacific SST changes (Lyon and DeWitt, 2012; Lyon, 2014; Yang et al., 2014) which have been primarily caused by natural Pacific Decadal Variability (PDV: Lyon et al., 2013); this research finds weak relationships between EA MAM rainfall and SST, and suggests that natural variations like the Pacific Decadal Oscillation (PDO) have played the primary role in reducing the East African long rains. A third perspective would acknowledge the important (dominant) role played by Pacific SST, but would interpret those SST variations as an interaction between anthropogenic warming in the western equatorial Pacific (WEP) and western North Pacific (WNP), El Niño/Southern Oscillation (ENSO) and PDV Hoell and Funk, 2013b; Funk and Hoell, 2015; Hoell et al., 2017b). Western Pacific warming is thought to increase influence of La Niña SST (Williams and Funk, 2010; Hoell et al., 2013; 2014; Hoell and Funk, 2013b), and an associated increase in the strength of the Indian Ocean branch of the Walker Circulation may explain the recent marked increase in correlation between observed MAM rainfall and SST (Liebmann et al., 2014; 2017). WEP influences are thought to provide one mechanism linking consecutive poor OND and MAM rainy seasons (Hoell and Funk, 2013a). Recognition of the emergent La Niña teleconnection (Williams and Funk, 2010) helped FEWS NET to provide effective early warning for the 2010/2011 EA drought (Hillbruner and Moloney, 2012). Furthermore, recognition of the

^aBurundi, Kenya, Rwanda, Somalia, Uganda.

^bLesotho, Madagascar, Malawi, Mozambique, Zambia, Zimbabwe, South Africa, Botswana, Swaziland. http://www.fews.net/global/alert/june-2017.

RMetS

TABLE 2 Selected SST regions and related drought-producing mechanism

Rainfall season/region	SST region	Lat/Lon	Influence of strong events
SA DJF	Niño 3.4	5°S-5°N 170°W-120°W	Triggers reorganization of Indo-Pacific Walker Circulation. Southern Indian Basin SST warm and low-level winds change, reducing onshore moisture transports into SA. Rainfall declines over SA.
EA OND	WEP	15°S–20°N 120°E–160°E	Warm WEP extremes associated with stronger Walker Circulation and strong IOD-like westerly wind anomalies over the eastern equatorial Indian Ocean. Reduced onshore moisture transports and rainfall over EA.
EA MAM	WNP	10°N-30°N 130°E-170°W	Western-V like SST pattern increases subsidence and trade winds over the equatorial central Pacific. Indian Ocean branch of the Walker Circulation intensified. Rainfall decreases over eastern equatorial EA.

important role played by western Pacific SST and the West Pacific Warming Mode (Funk *et al.*, 2014; Funk and Hoell, 2015; 2017) formed the basis of effective predictions of the 2016 OND and 2017 MAM droughts (Funk, 2016; Funk *et al.*, 2016a; 2016b).

EA OND rains have received substantially more historical analyses. Numerous studies have shown that EA OND rains correlate with ENSO (Ropelewski and Halpert, 1987; Ogallo et al., 1988; Nicholson and Kim, 1997; Indeje et al., 2000; Bretherton and Park, 2009), and this perspective dominated early research into OND interannual variability. As discussed in Nicholson (2017), this perspective was broadened in the late 1990s (Goddard and Graham, 1999; Saji et al., 1999). Saji et al. identified the Indian Ocean Dipole (IOD), based on the contrast between eastern and western equatorial Indian Ocean SST. Numerous articles have identified the link between IOD and EA rainfall (Clark et al., 2003; Behera et al., 2005; Ummenhofer et al., 2009; Nicholson, 2015; 2017). The leading mode of interannual variability is associated with ENSO/IOD co-variability (Bowden and Semazzi, 2007). Analysis by FEWS NET scientists has also stressed the important role of WEP SST in enhancing recent EA OND droughts, and suggested that warm western Pacific SST might provide a common and causal link between consecutive OND and MAM droughts (Hoell and Funk, 2013a).

There is a strong negative connection between El Niño's and southern African (SA) rainfall (Jury et al., 1994; Nicholson, 1997; Nicholson and Kim, 1997; Reason et al., 2000; Misra, 2003; Ratnam et al., 2014; Hoell et al., 2015; 2017a). El Niño events can reduce moisture convergence and vertical ascent, reducing tropical-extratropical cloud band development (Ratnam et al., 2014). Moisture convergence, driven by the Angolan Low and the Mascarene High in the south Indian Ocean supports the south Indian Ocean Convergence Zone (SIOCZ) and transports of moisture into SA. El Niño influences Indian Ocean basin SST and moisture transports (Nicholson, 1997; Reason et al., 2000; Ratnam et al., 2014), affecting southern African precipitation. SA precipitation is also influenced by the IOD (Saji and Yamagata, 2003) and the Subtropical Indian Ocean Dipole (SIOD: Behera and Yamagata, 2001; Hoell et al., 2017a); out-of-phase relationships between the SIOD and ENSO can act to enhance (reduce) El Niño influence over SA.

In general, there has been little research exploring the possible food security implications of seasonal covariations of the ENSO and western Pacific SST. Funk and Hoell (2015, 2017) for example, analyse ENSO and the ENSO-residual empirical orthogonal function (EOF) of global SST, which they describe as the West Pacific Warming Mode (WPWM). By construction, the WPWM is orthogonal (independent) of ENSO. Here, we use regional SST averages (Table 2) in the Niño 3.4, WEP and WNP to both explore rainfall and circulations variations associated with individual extreme seasons (our primary focus). As discussed below, SST in the WEP and WNP regions are modulated by ENSO, the IOD, anthropogenic forcing and PDV (Mantua and Hare, 2002; Lyon et al., 2013). Since WEP and WNP co-vary with ENSO, warming when the eastern Pacific cools, we are also exploring co-varying ENSO-western Pacific climate states. We briefly explore multi-year covariations in these SST indices, since they may in succession produce multi-year climate disruptions, such as the 1997/1998 El Niño and the long 1999-2001 period of drought producing La Niña-like climate that followed (Hoerling and Kumar, 2003).

Note that for all of our regions/seasons, past research has demonstrated important linkages to the Atlantic, Indian and Pacific basin SST and the ENSO, IOD, SIOD, PDO and other mechanisms. A thorough analysis of climate variability across these regions/seasons is beyond the scope of a single article. Our goal here is more limited, seeking to explore the role of extremely warm Indo-Pacific SST in recent African droughts.

2 | METHODS AND DATA

2.1 | Observational datasets

We use four observational datasets: a long time series of observed Extended Reconstruction version 4 (ERv4) SST (Huang *et al.*, 2015), a shorter set of blended gauge/satellite rainfall estimates – the Climate Hazards Group Infrared Precipitation with Stations (CHIRPS: Funk *et al.*, 2015b), along

with two long gauge-only precipitation datasets: the Global Precipitation Climatology Centre (GPCCv6: Becker *et al.*, 2013) and the Centennial Trends precipitation archive (Funk *et al.*, 2016b).

2.2 | Climate model simulations

We augment the observations with two types of simulations - SST-driven Atmospheric Model Intercomparison Project (AMIP) and fully-coupled Atmosphere-Ocean General Circulation Models (AOGCMS). Both the AMIP and fully-coupled simulations examined here are also constrained by observed changes in greenhouse gases, aerosols, and solar insolation. This study benefits from access to two large ensembles of 20 Community Atmosphere Model version 5.1 (CAM5) simulations (Neale et al., 2012) and 40 Community Earth Systems Model version 1 (CESM1) Large Ensemble Community Project (LENS) (Kay et al., 2015) simulations, made available by the Earth Science Research Laboratory's Facility for Climate Assessments (FACTS). While we also briefly examine additional AOGCM simulations (Table 3), we primarily focus on the CESM1 LENS simulations since this project provides a large ensemble that uses the CAM5 model. The CESM1 Large Ensemble Project is a set of climate model simulations intended for assessments of climate change in the presence of internal climate variability (Kay et al., 2015). CESM1 LENS provides 40 model simulations for 1920-2100 climate wherein the "butterfly effect" of small differences in initial state are allowed to propagate through the 1-degree version of the CESM1/CAM5 modelling system using historical and radiation concentration pathway (RCP) 8.5 external forcing (Taylor et al., 2011).

The difference between the AMIP CAM5 and AOCGM fully-coupled CESM1 LENS simulations is primarily due to how the ocean changes over time. In the CAM5 simulations, SSTs are prescribed based on a single historical record, so variations in circulation represented by the ensemble mean are fundamentally tied to oceanic forcing. We can contrast extremes from the early and later part of this observational record to explore potential circulation changes associated with extreme SST states. These analyses, however, face two limitations: small sample sizes and the potentially confounding effects of climate change and natural decadal variability.

To help overcome this limitation, we look for confirmation from the CESM1 LENS simulations. In the fully-coupled CESM1 LENS simulations, the CAM5 model is coupled to models representing the ocean, land and sea ice components of the climate system. These components interact, and the CESM1 LENS outputs represent multiple realizations of the climate system. The simulated SSTs from the fully-coupled CESM1 LENS are thus different from observations. In addition to our singular observed climate, we now have 40 alternative "realities." We examine extremes across the 40 CESM1 LENS simulations from 2000 to 2016, and

TABLE 3 Climate change models used for multi-model analysis

8	-
Modelling group and model name	Model acronym
Commonwealth Scientific and Indus- trial Research Organisation, Australia and Bureau of Meteorology, Australia	ACCESS-1.0
Canadian Centre for Climate Modelling and Analysis	CanESM2
National Center for Atmospheric Research	CCSM4
Community Earth System Model Contributors	CESM1-CAM5
Centre National de Recherches Météorologiques / Centre Européen de Recherche et Formation Avancée en Calcul Scientifique	CNRM-CM5
EC-EARTH consortium	EC-EARTH
The First Institute of Oceanography, SOA, China	FIO-ESM
NOAA Geophysical Fluid Dynamics Laboratory	GFDL-CMGFDL-ESM2G
NASA Goddard Institute for Space Studies	GISS-E2-H
Met Office Hadley Centre	HadGEM2-ES
Institut Pierre-Simon Laplace	IPSL-CM5A-LR
Atmosphere and Ocean Research Insti- tute (The University of Tokyo), National Institute for Environmental Studies, and Japan Agency for Marine–Earth Science and Technology	MIROC5
Max-Planck-Institut für Meteorologie (Max Planck Institute for Meteorology)	MPI-ESM-LR

look for similarities between these results and our CAM5 analyses. Note that we are primarily using the CESM1 LENS simulations as a large simulation archive to explore the impacts of natural variations within stationary climate conditions similar to those in the early twenty-first century. We also briefly examine climate changes in CESM1 LENS SST and SST from 14 fully-coupled climate change simulations (Table 3) obtained from the Climate Explorer (https://climexp.knmi.nl). This multi-model ensemble allows us to compare the observed SST changes with simulations from multiple modelling systems.

2.3 | Study questions

Using observations, CAM5 and CESM1 LENS simulations we explore three sets of interrelated questions:

- 1. What were the factors in 2015/2016/2017 relating unusually warm Indo-Pacific SST to recent SA and EA droughts? In what regions of the Indo-Pacific do we find robust relationships with EA and SA rainfall? What CAM5 circulation features seem to be associated with unusually warm SST in these forcing regions?
- Contrasting warm events in 1981–2016 and 1921–1980, do AMIP simulations indicate an increase in diabatic forcing and circulation anomalies conducive to SA/EA

droughts? Do contrasts between strong and moderate events in the fully-coupled CESM1 LENS 2000-2016 simulations also show increases in diabatic forcing? If so, this would indicate a limited role of decadal variability in the historical CAM5 changes. Do 2000-2016 CESM1 LENS simulations suggest that strong warm events are becoming more frequent?

3. Does it appear likely that moderate-to-strong El Niño's, followed by La Niña-like climate conditions, and associated droughts, might be a recurrent risk pattern for humanitarian agencies? Do these results indicate risks of back-to-back EA droughts?

2.4 | Examining CAM5 circulation features associated with unusual (1-in-6) warm events

Our approach to Question 1 is to composite SST for recent drought years, and identify areas where warm SST are associated with SA/EA droughts, those regions being Niño 3.4, WEP and WNP (Table 2). We then identify "unusually warm" seasons based on the warmest 1981-2016 1-in-6 Niño 3.4/WEP/WNP values. The 1-in-6 year frequency was used because it corresponds to moderate-to-strong El Niño events and a return period typical of severe SA and EA droughts. The 1-in-6 frequency selection was developed in our previous analyses attribution studies focusing on the 2015-2016 El Niño (Funk et al., 2016a; 2016b; 2018). It is well-established that El Niño events occur with a 3-to-7 year periodicity. Selecting 1-in-6 year warm events provides a simple means of identifying extremes without requiring the specification of specific SST thresholds - which can be difficult when comparing across multiple model simulations in a non-stationary changing climate. The work presented here shows that this approach can also be meaningfully applied to west Pacific SST extrema as well.

Once extreme seasons have been identified, CAM5 simulations are then used to identify the large-scale circulation features associated with these events. We examine whether unusually warm Niño 3.4/WEP/WNP SST appear associated with large-scale climate disturbances and SA/EA droughts. Do very warm WEP and WNP SST conditions, in addition to better known climate drivers such as La Niña, the IOD (Saji et al., 1999) or the Subtropical Indian Ocean Dipole (SIOD: Behera et al., 2000), appear associated with large circulation anomalies? This may be relevant to forecasting applications. During OND of 2016, Niño 3.4 and IOD anomalies were only weakly negative (Table 4), yet severe EA droughts led to major food insecurity (FEWSNET, 2017a; 2017b). During MAM of 2017, Niño 3.4 and IOD index values were positive (Table 4), indicative of above normal rainfall for East Africa (Hoell and Funk, 2013a), yet EA experienced a severe MAM drought event.

TABLE 4 DJF, OND and MAM SST index values

	Niño 3.4	SIOD Index	IOD Index	WEP or WNP
DJF 2015/2016	+1.80	-0.34	-0.32	
OND 2016	-0.57	+0.12	-0.20	+0.53
MAM 2017	+0.27	+1.2	+0.75	+0.40

Note. Expressed as standardized anomalies using a 1981-2010 baseline

2.5 | Examining changes in unusually warm (1-in-6) events with CAM5

The magnitude of Niño 3.4/WEP/WNP SST during unusually warm (1-in-6) events is increasing over time. The dynamic impacts of these changes are evaluated by (a) identifying unusually warm (1-in-6) events from the early (1921–1980) and late (1981–2016) part of the historical record, and (b) examining statistically significant (p < .05) CAM5 circulations changes between the 1981-2016 and 1921-1980 unusually warm seasons. We pick 1921 as a starting year because eastern equatorial ship-track data are sparse prior to that time (Funk and Hoell, 2015, supplemental material). This starting date also aligns well with the beginning of the CESM1 simulations. We then divide the 96-year observational record into 60- and 36-year periods, during which we identify 10 and 6 unusually warm (1-in-6) events. While somewhat arbitrary, the 1921–1980 versus 1981–2016 division is supported by a stronger (weaker) anthropogenic warming signal after (before) 1980 in the two main modes of global SST variability - ENSO and WPWM (Funk and Hoell, 2015). An examination of 1921-2016 Pacific Decadal Oscillation values (Mantua and Hare, 2002) indicates that these two epochs are essentially neutral and equal, in terms of the PDO (not shown). Two sets of two-sided statistical t-tests are used to identify significant (p < .05) changes in the 1981–2016 and 1921-1980 CAM5 precipitation and 850 and 200 hPa circulation fields. Each t-test contrasts a 1981–2016 sample comprising 120 members (6 extreme seasons x 20 CAM5 simulations) and a 1921-1980 sample composed of 200 members (10 extreme seasons x 20 CAM5 simulations).

2.6 | Examining changes in strong and moderate warm events using the CESM1 LENS ensemble

The 40 CESM1 LENS simulations are used to examine the difference between "moderate" and "strong" warm events over the 2000-2016 time period. Thresholds for moderate and strong warm events are defined based on the observed Niño 3.4/WEP/WNP time series, using the 1921-1980 and 1981-2016 time periods. For example, strong El Niño's are defined as those with standardized Niño 3.4 SST anomalies of more than +1.7Z, while moderate El Niño's have Niño 3.4 SST anomalies ranging from +0.5Z to +1.7Z. Z is used here to denote one standard deviation. Samples of strong and moderate events are identified, and two-sided

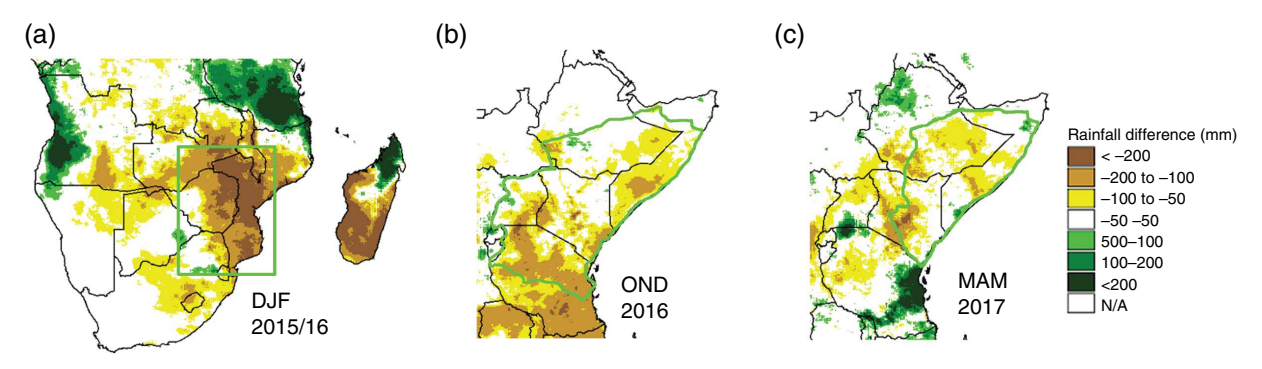


FIGURE 1 CHIRPS rainfall anomalies for (a) DJF 2015/2016, (b) OND 2016, and (c) MAM 2017

t-tests are used to identify significant (p < .05) changes in strong *versus* moderate CESM1-simulated SST and precipitation fields. While similar to the CAM5 results, the CESM1 LENS analysis provides us with a much larger sample of SST states ($40 \times 17 = 680$ years, as opposed to 96 years for the 1921–2016 observations) and a means of controlling for both natural and external decadal variability.

2.7 | Potential convergence of evidence

To summarize, links between Niño 3.4/WEP/WNP SA December–February (DJF), EA OND, and EA MAM rainfall are evaluated based on (a) SST composites for recent dry seasons, (b) out-of-sample (cross-validated) regressions, (c) CAM5 composites for 1981–2016 unusually warm seasons, (d) changes between CAM5 1981–2016 and CAM5 1921–1980 composites, and (e) changes between CESM1 LENS composites during 2000–2016 strong and moderate warm events.

2.8 \mid Methods for exploring multi-year increases in drought

Multi-year drought sequences and associated food crises present significant challenges to disaster risk management. We examine time series of observed and simulated SST (Table 3) to quantify the frequency of alternating Niño/Niña-like SST patterns. We use the term "La Niña-like" to refer to climate conditions associated with an enhancement of the Walker circulation and west-versus-east Pacific SST gradients. West-versus-east Pacific SST gradients may produce La Niña-like disruptions in the absence of a fully developed La Niña. WEP and WNP warming may play an important role in the generation of such gradients and circulation responses. These may occur in sequence, initiated by an El Niño and potential droughts in Ethiopia and SA, and then followed by a La Niña-like climate state associated with cool eastern Pacific SST, warm western Pacific SST, and potential droughts in EA. This may result in several years of increased interventions, similar to that experienced in 2016/2017 (Table 1).

3 | RESULTS

3.1 | Relating recent droughts to SST extrema

Here we evaluate recent SA DJF, EA OND and EA MAM droughts. Figure 1 shows CHIRPS precipitation anomalies for DJF 2015/2016, OND 2016, and MAM 2017 and polygons that outline the rainfall regions examined. We use CHIRPS as our primary African observational data set because (a) the CHIRPS incorporates a greater number of station data for southern Africa, Somalia and Ethiopia, and (b) CHIRPS data are available through to May of 2017. In general, seasonal CHIRPS rainfall performance is similar to the GPCC (Funk et al., 2015b). The box shown in Figure 1a was based on the region with the highest DJF rainfall (CHIRPS) correlation with Niño 3.4 SST (Funk et al., 2016a; 2016b). The regions drawn in Figure 1b,c represent homogenous areas that tend to exhibit coherent EA droughts. OND droughts tend to be more spatially coherent than those in MAM (Lyon, 2014).

We extend these precipitation time series back to 1921 using Centennial Trends precipitation data for EA and GPCC data for SA. The correspondence between these data sources for the seasonal regional accumulations was very high: DJF CHIRPS/GPCC correlation = 0.92, OND CHIRPS/Centennial Trends correlation = 0.99, MAM CHIRPS/Centennial Trends correlation = 0.92. CHIRPS data was used from 1981, and prior values were estimated via regressions with GPCC or Centennial Trends data. For EA, the CHIRPS and Centennial Trends datasets benefit from a fairly large number of additional stations, obtained from national meteorological agencies and the Florida State University archives (Funk *et al.*, 2016b).

3.2 | Using drought composites and correlations to identify SST forcing regions

To explore the contemporaneous relationship between SST and drought in these regions, we identified the six driest seasons since 1981. Figure 2a–c show composites of contemporaneous ERv4 SST, screened for significance at p < .1, based on two-sided t-tests. We also plotted the

RMetS

correlation between our African precipitation time series and contemporaneous rainfall of the last 20 years (Figure 2d–f). We chose to use this shorter time period to guide our selection process because (a) our focus here is on informing improved forecasting and monitoring for the next several SA or EA droughts, thus we are primarily interested in predicting droughts under circumstances similar to current conditions, and (b) the EA MAM rainfall-SST relationship appears to have increased substantially over the past 20 years, presumably due to a stronger Indian Ocean branch of the Walker Circulation (Liebmann et al., 2014; 2017). Table 5 lists 1977-1996 and 1996-2016 rainfall correlation values for Niño 3.4, IOD and western Pacific SST. For Niño 3.4/DJF, WEP/OND and WNP/MAM, the 1997-2016 correlations are all close to -0.7. Note that the IOD/OND correlation is very strong (+0.9). This would be the best predictor. Here, however, we analyse WEP SST, because we are primarily interested in the potential role that warm WEP SST plays in supporting consecutive OND/MAM droughts (Hoell and Funk, 2013a). Such a concern also guides our selection of Niño 3.4 versus the Indian Ocean region for DJF; we are interested in exploring El Niño-La Niña sequences.

Based on Figure 2a-f we selected Niño 3.4, the WEP and WNP regions for DJF, OND and DJF as regions where warm SST is associated with African drought (Table 2). This selection procedure was based on (a) areas in Figure 2a-c that exhibited statistically significantly above-normal SST in regions identified in the literature as important, and (b) areas that exhibited significant negative correlations (Figure 2d-f). By this selection, we do not mean to imply that other regions do not influence SA and EA regions. Our goal here is to explore the impacts of unusually warm Indo-Pacific SST. Note that the DJF correlation maps also highlight strong negative relationships in the Indian Ocean, while the OND and MAM correlation maps also identify significant positive relationships in the Indian and east Pacific Oceans. All these regions will be influenced by ENSO, and many will also be affected by the IOD. It is beyond the scope of this study to disentangle these influences across three different seasons, nor is it necessary for our purpose – which is to explore what happens when the Niño 3.4, WEP and WNP are exceptionally warm, with the understanding that ENSO, decadal variations, warming trends and other processes all likely contribute to creating these warm events.

Figure 2g–i underscore this point by showing observed DJF 2015/2016, OND 2016 and MAM 2017 SST, standardized using 1981–2010 SST. When examining these panels, it is important to realize that a +1.5Z threshold represents unusually warm ocean conditions, so the large coverage of red areas in these panels is likely to be an expression of rapid warming. The 2015/2016/2017 DJF/OND/MAM droughts (Figure 1) were accompanied by exceptionally warm SST (Figure 2g–i).

TABLE 5 Correlations between indices and African precipitation

	1977-1996	1997–2016
SA DJF P and NINO34 SST	-0.57	-0.74
EA OND P and WEP SST	-0.58	-0.75
EA OND P and NINO34 SST		+0.61
EA OND P and IOD SST	+0.51	+0.90
EA MAM P and WNP SST		-0.70
EA MAM P and Niño 3.4 SST		+0.54
EA MAM P and IOD SST		

Note. Values not significant at p < .05 not shown.

3.3 | Historical context of the 2015/2016/2017 DJF/OND/MAM droughts

The history of rainfall in these regions, and placement of the 2015/2016/2017 DJF/OND/MAM droughts in that context, are now discussed. Figure 3a-c present long (1900-2016) time series of SA DJF, EA OND and EA MAM rainfall expressed as Standardized Precipitation Index (SPI) anomalies (McKee et al., 1993), based on Gamma distributions (Husak et al., 2007) and a 1900-2016 baseline. For SA DJF, the 2015/2016 drought was among one of the worst in the 36-year CHIRPS record and among the 10 driest DJF seasons since 1900. The SA DJF time series appears relatively stationary, although there have been relatively few (two) years since 2000 with rainfall within the upper tercile (standardized rainfall anomalies $\geq +0.5Z$): 2004 and 2006. EA OND rains, on the other hand, indicate a strong propensity towards above-normal rainfall: 10 events since 1997 have had above-normal rainfall (SPI>+0.5Z). MAM rains, however, have declined substantially (Funk et al., 2005; 2015a). In the 27 years since 1991, only three seasons (1997, 2010, 2013) have had good rains (standardized anomalies > +0.5Z).

3.4 | Evaluating SST regions as potential predictors of drought: DJF (Niño 3.4), OND (WEP), MAM (WNP)

We next examine take-one-away cross-validated (Michaelsen, 1987) estimates of SA and EA rainfall based on our SST regions. We do this for the past 20 years to emphasize the potential utility of these regions for predicting severe droughts. While not a true forecast, since we are using contemporaneous SST values, these scatterplots project reasonable skill in identifying recent severe droughts.

For SA DJF (Figure 3d), most, but not all, recent droughts occur along with positive Niño 3.4 SST, and a 2015/2016 forecast based on Niño 3.4 SST would have correctly predicted the drought, though underestimated the intensity, probably because some strong El Niño's (1997/1998) have not been associated with large droughts and some strong droughts (2001/2002) have not been associated with El Niño's.

For EA OND (Figure 3e) we find a fairly robust linear univariate relationship, with the wettest events well delineated.

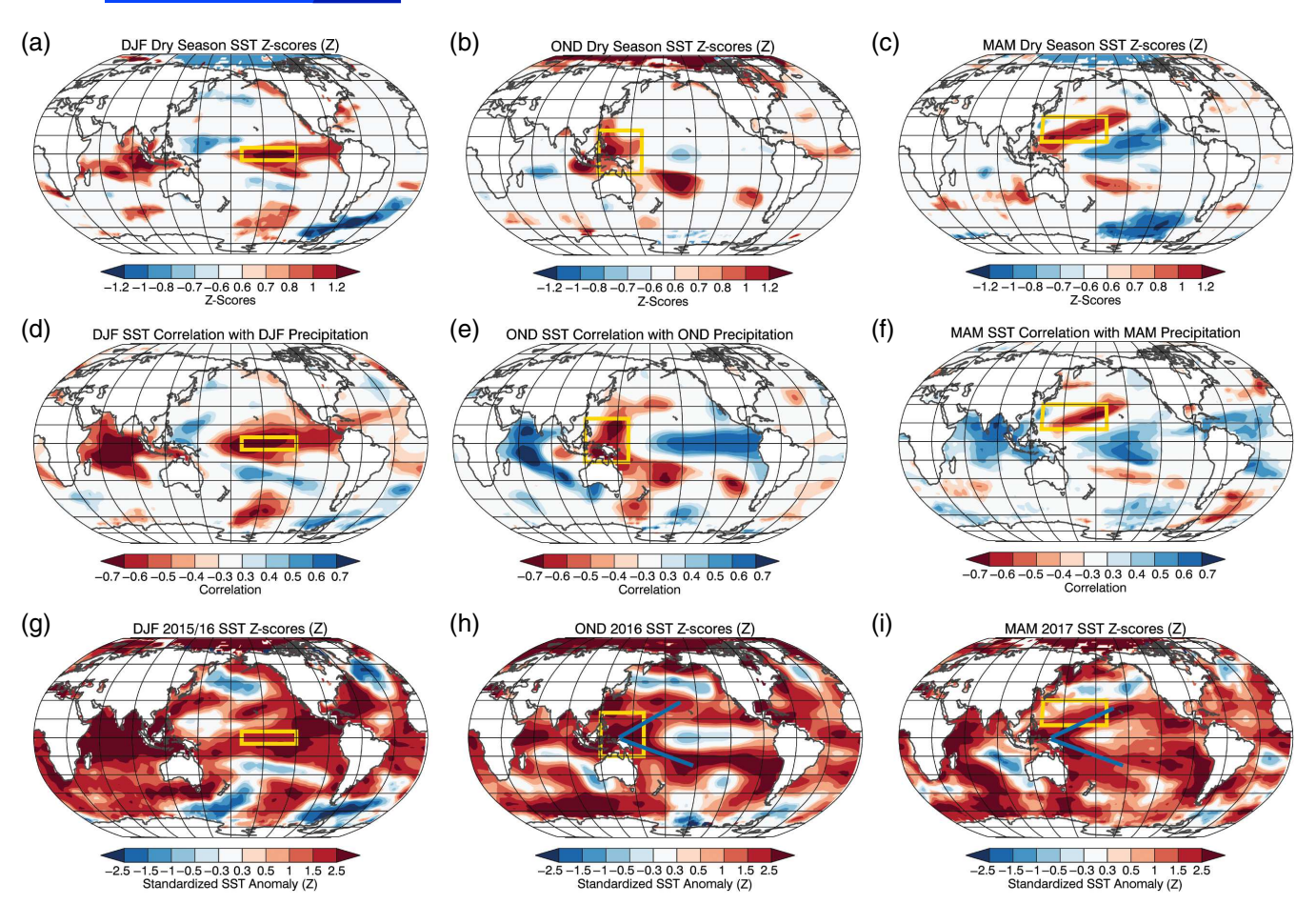


FIGURE 2 (a–c) Composites of standardized seasonal SST for the six driest seasons between 1981 and 2016. Values not significant at p < .1 have not been coloured. DJF dry seasons: 1991/1992, 1982/1983, 2015/2016, 1986/1987, 2001/2002 and 2002/2003. OND dry seasons: 2005, 1998, 1996, 1993, 2010 and 2016. MAM dry seasons: 2011, 1984, 2000, 2009, 1999 and 2004. (d–f) 1997–2016 SST correlations with contemporaneous regional African rainfall. Values not significant at p < .1 have not been coloured. (g–i) 2015/2016/2017 standardized SST anomalies. All anomalies based on a 1981–2010 baseline

The most severe droughts (2016, 2010, 1998 and 2005) are predicted to be below normal, but the magnitude of the 2005 and 1998 events are not reproduced well. The year 2005 appears associated with a substantial "Western V"-like SST anomaly pattern, but with the equatorial western Pacific displaced eastward to centre on 170°E (not shown). The 1998 OND season was associated with a strong La Niña event.

For EA MAM (Figure 3f), WNP SST-based predictions have a relatively low R2 value, but correctly identify all the recent droughts. All the recent droughts occur with consistently warmer SST in the western Pacific and thus high WNP values appear to be a robust indicator of poor EA MAM rainfall performance. Many of these high WNP/low EA MAM rainfall events follow antecedent El Niño's (Figure 3g). The 1997/1998 El Niño is followed by poor MAM rains and high WNP in 1999, 2000 and 2001. The 2002/2003 El Niño is followed by poor 2004 MAM rainfall. The 2006/2007 El Niño is followed by the EA MAM droughts of 2008 and 2009. The 2009/2010 El Niño is followed by the 2011 EA drought and high WNP SST. The 2015/2016 El Niño is followed by the 2017 EA MAM drought and high values of WNP SST. Many of these El Niño events are followed by warming in the WNP and concurrent drought the following MAM.

3.5 | Identifying 1921–1980 and 1981–2016 1-in-6 warm events

We next examine the 1921–2016 time series of Niño 3.4, WEP and WNP SST (shown in Figure 3g–i). Our objective is to identify 1921–1980 and 1981–2016 1-in-6 extreme events so that we can use these events as the basis for CAM5 composites. The distribution of these values will also be used to identify temperature thresholds associated with "moderate" and "strong" events, to support our analysis of the CESM1 LENS ensemble, as described in our methods section. To facilitate the CESM1 LENS analysis, we present standardized SST indices.

For all three regions, we find statistically significant (p < .01) increases in the observed ERv4 means of the 1981–2016 *versus* 1921–1980 1-in-6 year maxima (Table 6). Similar increases are also found in 53 different climate change simulations, consistent across models (Table 7). While the WEP and WNP time series exhibit strong non-stationarities that are likely to be related to anthropogenic warming (Funk and Hoell, 2015; 2017), the high variability (Wittenberg, 2009) and limited accuracy (Solomon and Newman, 2012) of east Pacific SST makes such an identification difficult for the Niño 3.4 region. It is very hard to assess Niño 3.4 changes

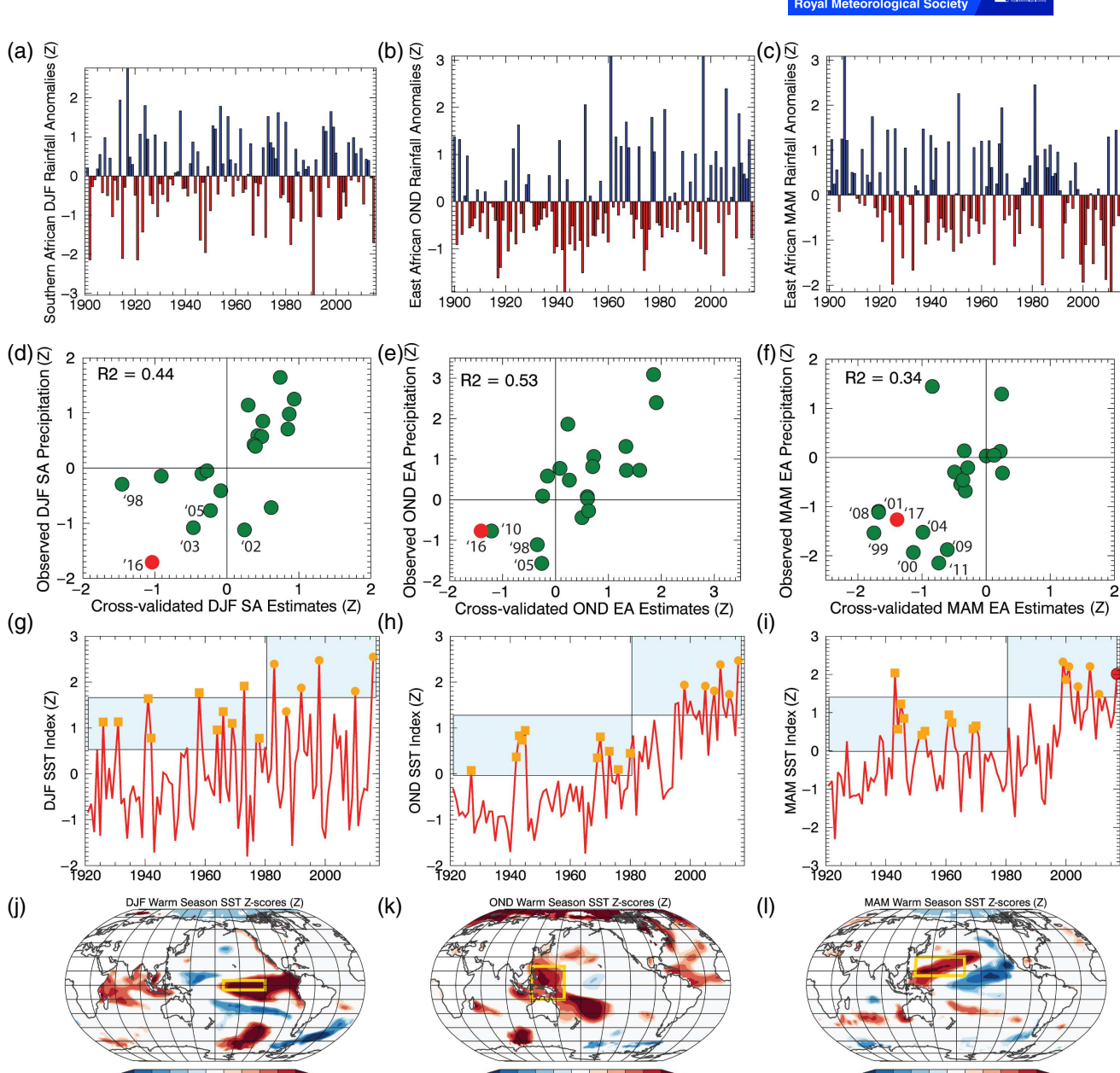


FIGURE 3 (a–c) Time series of SA DJF rainfall, EA OND rainfall and EA MAM rainfall, based on a 1900–2016 baseline. (d–f) Scatterplots of cross-validated rainfall estimates. (g–i). Time series of regional SST time series (Table 2). Boxes and squares identify pre- and post-1981 extrema. The 2017 MAM value is shown with a red circle. Rectangles identify SST ranges used in later analyses of CESM climate change simulations. (j–l) Standardized SST anomalies for the six 1981–2016 warm events (circles in g–i), based on a 1981–2010 baseline. Screened for significance at p < .1. Yellow rectangles denote the SST forcing regions analysed

-1.4 -1.2 -1 -0.9 -0.8 0.8 0.9

based on a single time series as in the case of the observed record. We address this issue by using the CESM1 LENS simulations. For MAM there is conformity between recent dry years being associated with warm WNP SST (Figure 3f) and the step-like increase in WNP SST after 1998 (Figure 3i). Thus the increase in west Pacific temperature seems like a plausible explanation for the recent abrupt (Lyon and DeWitt, 2012) MAM drying (Figure 3c). For OND, we notice an intriguing difference. Warm WEP OND SSTs are associated with drier EA outcomes (Figure 3e), and WEP SSTs have warmed steadily since the 1980s (Figure 3h), but OND rains do not exhibit a drying trend (Figure 3b). This is probably related to the large influence of the IOD (Table 5)

1.4 –1.2 –1 –0.9 –0.8 0.8 0.9

TABLE 6 1981–2016 and 1921–1980 1-in-6 year maximum SST means

-1.4 -1.2 -1 -0.9 -0.8 0.8 0.9

Region	1981–2016, 95% confidence based on std. errors	1921–1980 extrema, 95% conf.	Change 1981–2016 vs. 1921–1980	p value (two-sided t-test)
Niño 3.4 DJF	28.5940.18	27.840.16	+0.77C	.0036
WEP OND	29.4740.16	29.040.14	+0.48C	.0001
WNP MAM	26.5840.18	26.2940.14	+0.28C	.0001

and a positive influence associated with a warming Indian Ocean.

Note that we have also shown, with blue boxes in Figure 3g-i, ranges used in our CESM1 LENS analysis of diabatic forcing during strong *versus* moderately warm SST

TABLE 7 Change in 1-in-6 year extreme SST, by model

Model acronym	Number of simulations	Niño 3.4 DJF	WEPv OND	WNP MAM
ACCESS-1.0	1	+0.7Z	+1.3Z	+1.6Z
ACCESS-1.3	1	+0.6Z	+1.7Z	+.18Z
BCC	1	+1.4Z	+1.7Z	+1.7Z
CanESM2	5	+0.9Z	+1.8Z	+1.7Z
CCSM4	6	+0.8Z	+1.5Z	+1.6Z
CESM1-CAM5	2	+0.8Z	+1.3Z	+1.7Z
CNRM-CM5	5	+0.6Z	+1.0Z	+1.3Z
EC-EARTH	6	+1.1Z	+1.6Z	+1.3Z
FIO-ESM	3	+0.6Z	+1.7Z	+1.6Z
GFDL-CM	1	+0.7Z	+1.6Z	+1.7Z
GFDL-ES	2	+1.2Z	+1.2Z	+1.3Z
GISS-E2-H	3	+1.0Z	+1.1Z	+1.6Z
GISS-E2-R	3	+0.9Z	+0.9Z	+1.4Z
HadGEM2-ES	3	+0.6Z	+1.1Z	+1.4Z
INM-CM4	1	+0.5Z	+1.0Z	+1.4Z
IPSL-CM5A	3	+0.6Z	+1.5Z	+1.9Z
MIROC5	3	+0.5Z	+0.9Z	+1.1Z
MPI-ESM	4	+1.2Z	+1.7Z	+1.9Z
Total Ensemble	53	+0.8Z avg.	+1.7Z avg.	+1.6Z avg.
		+0.4Z std. dev	0.4Z std. dev	0.3Z std. dev

Note. 1981–2016 *versus* 1921–1980, based on standardized SST using a 1921–2016 baseline.

events. The horizontal line demarcating the vertical boundary between the two boxes is based on the midway point between the observed average 1981–2016 and 1921–1980 1-in-6 year maxima: $T_{\rm mid}=0.5(T_{1981-2016}+T_{1921-1980})$. Strong warm events in the CESM1 LENS simulations are defined as those warmer than $T_{\rm mid}$. Moderate warm events are less than $T_{\rm mid}$, but warmer than a bottom threshold ($T_{\rm bot}=T_{1921-1980}-1.8\sigma$), where $T_{1921-1980}$ and σ are estimated using the 10 1921–1980 warm event values. It should be noted that both the WEP OND and WNP MAM time series co-vary with Niño 3.4 SST. The contemporaneous correlation between WEP and Niño 3.4 OND SST has been -0.75 and -0.55 for the past 20 and 30 years. The corresponding correlations for MAM WNP are -0.70 and -0.61, respectively.

3.6 | Evaluating potential long-term SST drivers of MAM decadal rainfall: PDO, Niño 3.4, WNP

Figure 4 explores decadal reductions in EA MAM rainfall by plotting 10-year averaged EA MAM rainfall with 10-year averaged PDO, Niño 3.4 and WNP time series. The correlations between 1921 and 2016 10-year averaged EA MAM rainfall and the PDO and Niño 3.4 indices are weak (Figure 4, r = 0.23 and -0.12). The anti-correlation between 10-year EA MAM rainfall and 10-year WNP SST is substantially stronger (r = -0.63). Focusing on decadal co-variations after 1940, one finds an even stronger correlation WNP/EA (-0.83), with relatively cool WNP and wet EA conditions from $\sim 1945-1993$ followed by warming and drying in the WNP

and EA MAM time series. After 1993 the PDO decreases, Niño 3.4 SSTs decrease, and WNP SSTs increase, so it is very hard to disentangle these northern Pacific climate patterns. The decadal variations of WNP SST and EA MAM rainfall are at historic high and low values. Since the WNP region was defined based on recent drought years, it is interesting that it also performs well as a metric of decadal variability.

3.7 | CAM5 circulation anomalies during moderate-strong SST forcing regions events: 1981–2016

Here, we explore CAM5 circulations associated with the 1981–2016 unusually warm SST events (Figure 3j–l) associated with the seasons marked with circles in Figure 3g–i. Figure 3j is similar to a canonical ENSO pattern (Rasmusson and Carpenter, 1982) that extends across the eastern Pacific, a pattern associated with substantial drying over SA (Ratnam *et al.*, 2014; Funk *et al.*, 2016a; 2016b). Figure 3k identifies increased WEP SST and warmer conditions over the South Pacific Convergence Zone (SPCZ). As expected, Figure 3l identifies WNP warming, but also an interesting off-equatorial cool SST area to the southeast of Hawaii. We next explore the dynamic impacts of these SST patterns using 20 CAM5 simulations.

Figure 5 shows CAM5 anomaly composites of 1981–2016 warm events for precipitation and 850 hPa winds (Figure 5a,c,e) and 200 hPa geopotential heights and winds (Figure 5b,d,f). All results are based on a 1981–2010 baseline, screened for significance at p < .05.

As one might expect, the DJF Niño 3.4 composites (Figure 5a,b) clearly show large-scale circulation patterns typically associated with strong El Niño events: large (+2Z) increases in central Pacific precipitation and a large reduction in the speed of the central Pacific trade winds, accompanied by the formation of twin upper-level anticyclonic high-pressure cells over the eastern Pacific and a Pacific-North American (PNA) pattern response associated with a barotropic Rossby wave-train. ENSO events are thought to modulate SA climate through changes in the Africa-Indian Ocean Walker circulation cell and anomalous anticyclonic circulation over southern Africa and South Atlantic High Pressure cell (Reason et al., 2000), features which we see in Figure 5a,b. Over equatorial and southern Africa, the 850 and 200 hPa wind fields indicate the baroclinic response associated with a Matsuno-Gill type equatorial response to diabatic forcing and strong El Niño events (Hoell et al., 2015).

For OND (Figure 5c), the surface wind field over the eastern equatorial Indian Ocean identifies a strong westerly wind anomaly – a pattern identified as a very strong indicator of East African OND droughts (Hastenrath *et al.*, 2007), and an increase (decrease) in precipitation over the west (central) Pacific Ocean. We find increased subsidence at the dateline and a weak increase in easterly trades between 160°E

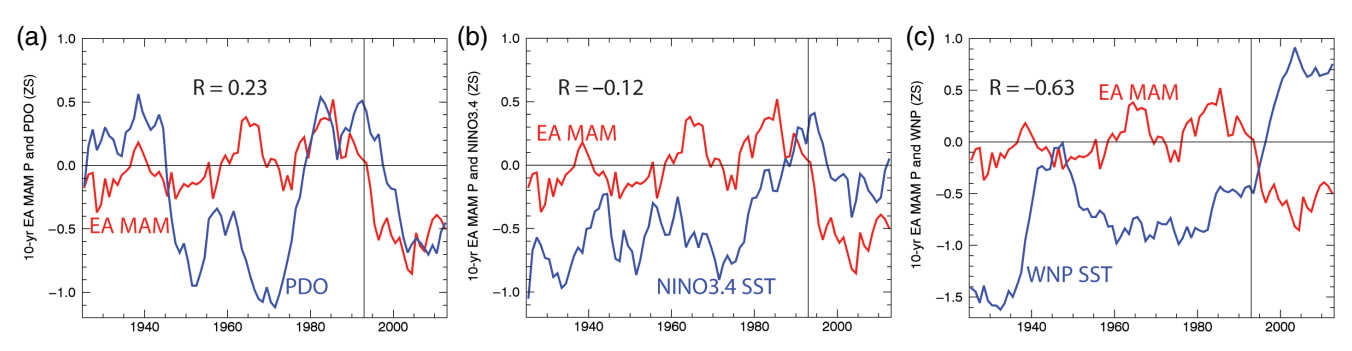


FIGURE 4 Time series of 10-year averaged EA MAM (red) and (a) PDO, (b) Niño 3.4 SST, and (c) WNP SST. Standardized data centred on a 1981–2010 baseline

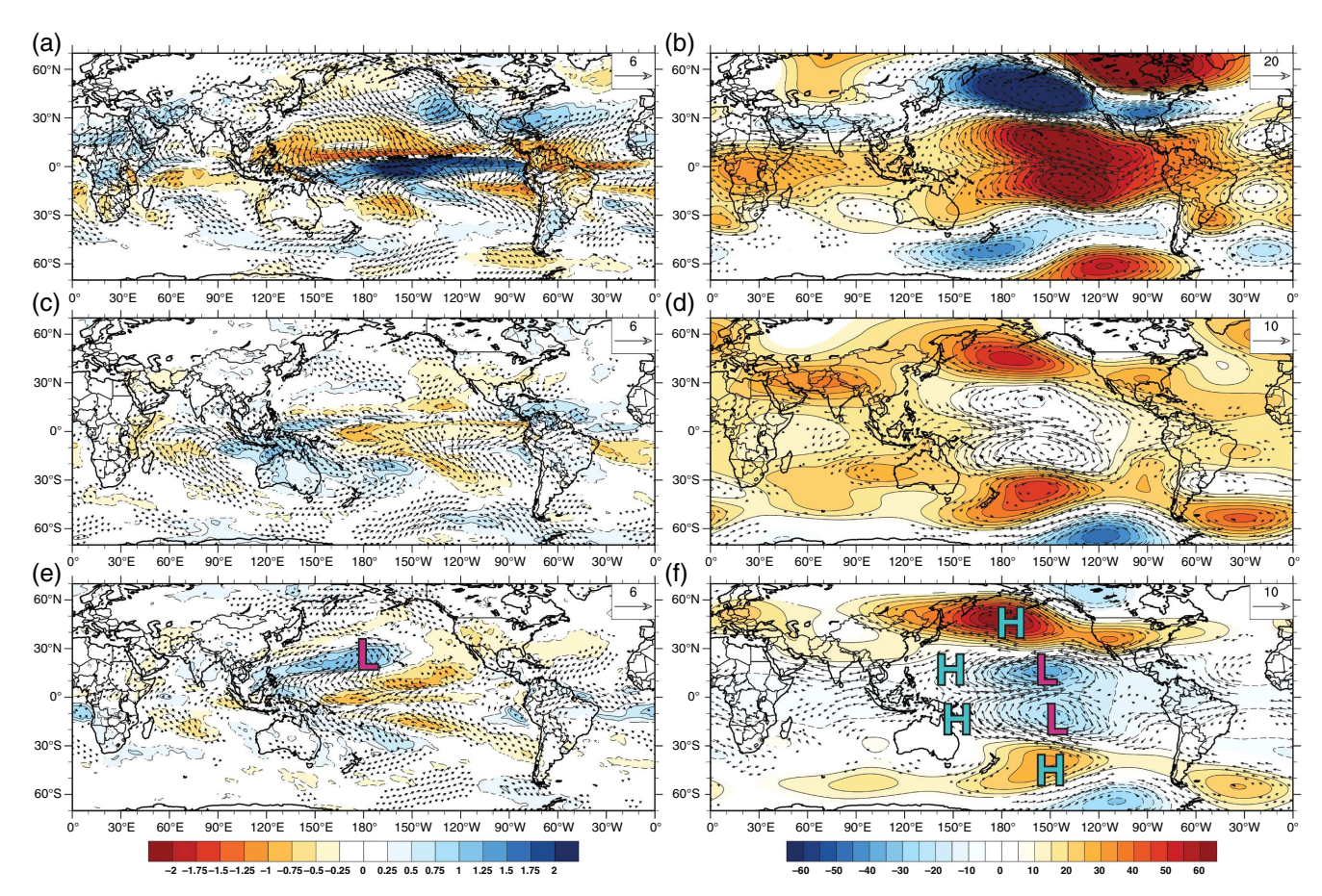


FIGURE 5 ESRL CAM5.1 composites for 1981–2016 warm events. (a) DJF precipitation Z-scores and 850 hPa wind anomalies. Precipitation field screened at p < .05. Black arrows show winds significant at p < .05. (b) Same as (a) but for 200 hPa heights and winds. (c–d) Same as (a) and (b) but for OND. (e–f) Same as (a) and (b) but for MAM. All anomalies based on a 1981–2010 baseline

and 150°W. In the upper troposphere we find twin cyclonic responses over the eastern Pacific, similar to a La Niña-like response, and an associated increase in upper-level easterlies over the tropical eastern Indian Ocean and westerly flows over the tropical central Pacific.

For MAM (Figure 5e,f) we find a strong (+1Z) enhancement in precipitation in the northwestern Pacific, and a fairly large decrease in equatorial precipitation from 150°E to 120°W. The increased WNP diabatic forcing (rainfall), cool off-equatorial east Pacific SST, and "Western V"-like warm SST anomalies stretching from the maritime continent to the north of Hawaii (Figure 31) appears conducive to the formation of paired upper-level cyclones near 150°W

15°S/N. These twin cyclones guide convergent upper-level winds over the central Pacific. Focusing on the zonal upper-level near-equatorial wind responses, Figure 5f identifies substantial intensification of both the Pacific and Indian Ocean branches of the Walker Circulation. Such a circulation change is thought to be associated with drier EA MAM conditions (Williams and Funk, 2011; Liebmann *et al.*, 2014; 2017), although this drying is not recreated by the CAM5 model.

Note that while both WEP OND and WNP MAM analyses indicate an intensification of the Walker Circulation, the OND upper-level responses are weaker, but characterized by a stronger IOD-like Indian Ocean wind response.

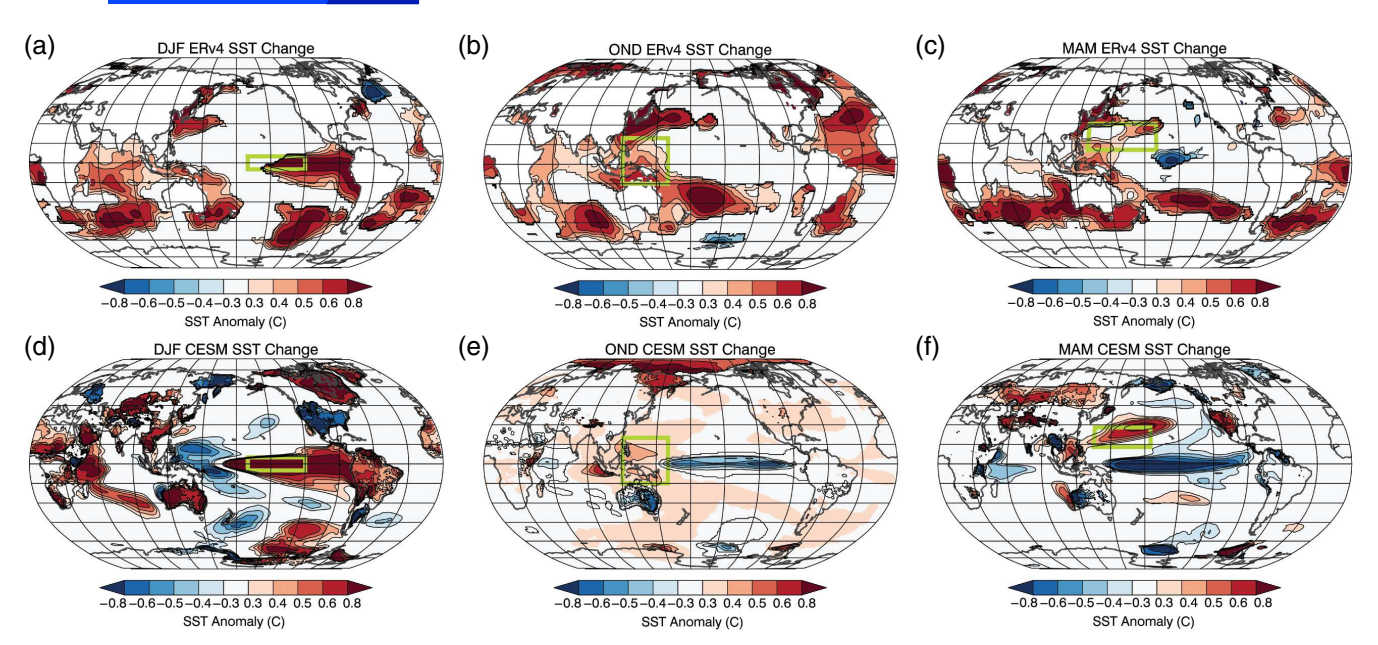


FIGURE 6 (a-c) Changes in ERv4 SST for 1-in-6 1981–2016 versus 1921–1980 warm events. (d-f) Composites of CESM1 LENS 2000–2016 surface temperatures anomaly difference for strong versus medium warm events

This section has explored a fairly simple but important point: recent SA and EA droughts, including those in 2015/2016/2017 have been associated with very warm SST in teleconnected regions of the Pacific Ocean. These warm SST events appear related to ENSO, Pacific Decadal Variability, and climate change, but detailed attribution of these events is not required for effective early warning. When these regions are very warm the risk of drought will likely be elevated. The robust contemporaneous estimation skill (Figure 2d-f) and the vigorous atmospheric response identified by the CAM5 (Figure 5) indicate good prospects for prediction. While many studies have examined the relation between El Niño and southern African drought, EA MAM predictability has generally been considered poor, with EA MAM rainfall having a weak relationship to SST (Lyon, 2014). The results presented here challenge that assumption, finding strong relationships between WNP SST and recent droughts (Figure 2f) and decadal rainfall variations (Figure 4c). While valid arguments for a weak MAM teleconnection can be made based on the weak 1981-2016 correlation between EA MAM rainfall and SST, this correlation has increased substantially in recent years (Liebmann et al., 2014), likely due to a strengthening of the Indian Ocean branch of the Walker Circulation (Funk et al., 2008; Williams and Funk, 2011; Liebmann et al., 2017). Another important aspect may be nonlinearities in EA MAM teleconnections; SST composites for the six 1981-2016 EA MAM wet seasons show no significant Indo-Pacific anomalies. Dry seasons do (Figure 2c).

3.8 | Exploring differences in climate responses to moderate and strong warm events

Figure 6a–c show observed (ERv4) SST differences for 1981–2016 and 1921–1980 1-in-6 warm events. Figure 6d–f

show differences between the CESM1 LENS SST fields associated with strong and moderate warm events, based on the SST ranges shown in Figure 3g–i. The observed differences in DJF SST identify significant warming in the eastern Pacific and Indian Ocean, as well as substantial warming in parts of the Southern Ocean, and cooling in the North Atlantic. The observed OND SST difference composite identifies warming in the WEP, off the coast of China, within the SPCZ, and in areas of the Southern Ocean and Atlantic. The observed MAM SST difference composites identify warming in the WNP, Southern Ocean, and equatorial Atlantic. In the Indo-Pacific, the DJF composite indicates a stronger El Niño response in the eastern Pacific and Indian Ocean. For OND and MAM we find a "Western V"-like response in the Pacific.

The CESM1 LENS DJF Niño 3.4 difference field for strong versus moderate warm events (Figure 6d) identifies substantially warmer SST over the eastern equatorial Pacific and Indian Ocean, and cooler SST near the maritime continent. The OND composite shows modest increases and decreases in WEP and central Pacific SST (Figure 6e). The MAM SST composite (Figure 6f) identifies substantial increases in SST to the northwest of Hawaii, and substantially cooler SST along the eastern equatorial Pacific. In the CESM1 LENS composites, the warmest WNP events in MAM, and to a lesser degree, OND, appear associated with La Niña-like SST patterns. It is worth noting the general similarity between Figure 6a-f and Figure 2a-f, which depict SST conditions associated with recent SA and EA droughts. Figure 6d-f suggest that strong CESM1 LENS warm events may be more conducive to SA/EA droughts than moderate events.

Figure 7 shows CAM5 difference composites, screened for significance at p < .05. The DJF Niño 3.4 rainfall/850 hPa wind composite (Figure 7a) identifies large increases in equatorial Pacific precipitation across the entire Pacific between

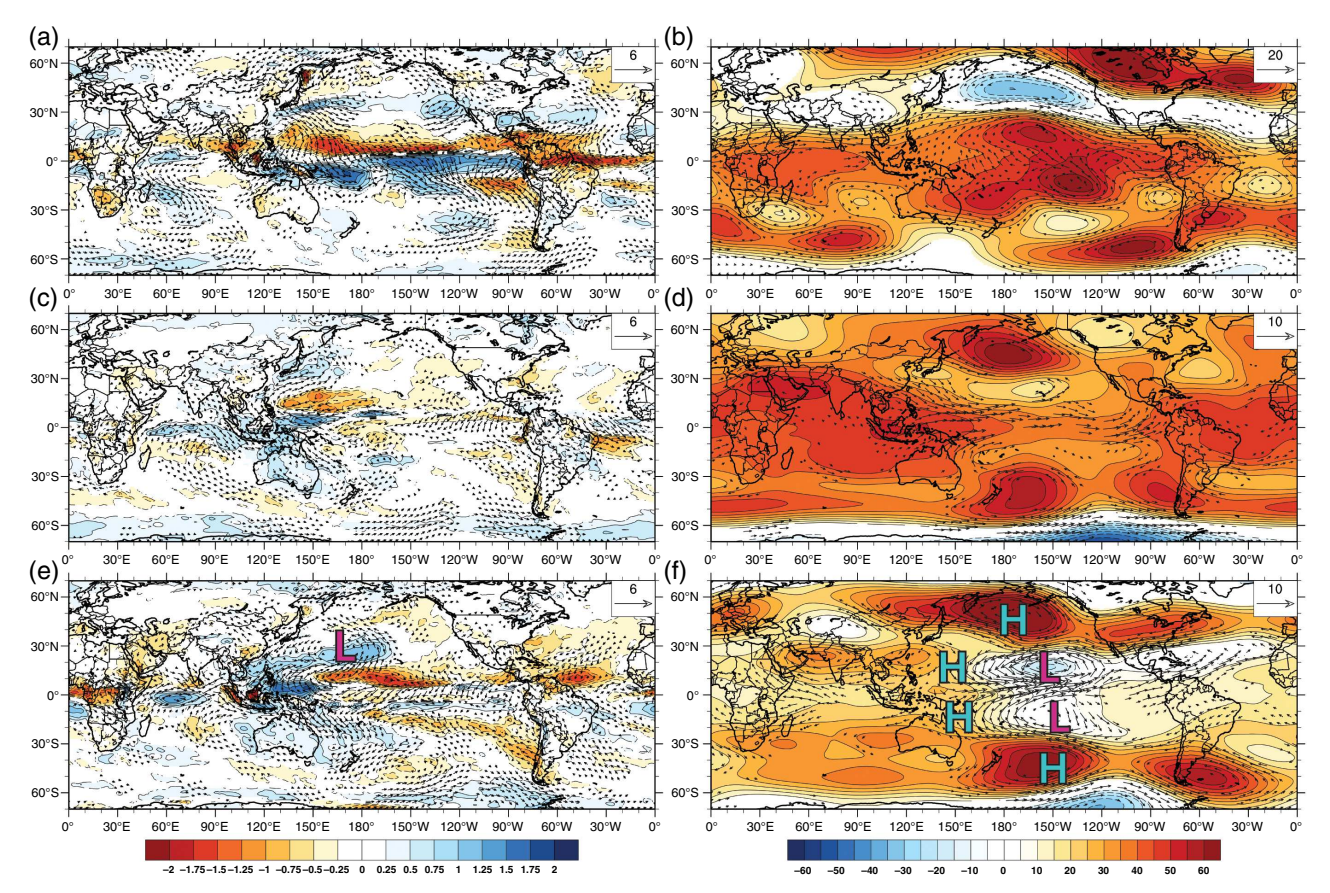


FIGURE 7 ESRL CAM5.1 composites for 1981–2016 warm events *versus* 1921–1980 warm events. (a) DJF precipitation Z-scores and 850 hPa wind anomalies. Precipitation field screened at p < .05. Black arrows show winds significant at p < .05. (b) Same as (a) but for 200 hPa heights and winds. (c–d) Same as (a) and (b) but for OND. (e–f) Same as (a) and (b) but for MAM

150°E and 90°W and large reductions across the maritime continent, tropical North Pacific, Central America, northern South America, and the equatorial Atlantic. A weaker but statistically significant decrease in rainfall is found over SA. The 850 hPa wind field shows westerly wind differences over the equatorial Pacific, consistent with weaker upwelling and warmer SST. Over the western Indian Ocean we find a westerly difference pattern associated with reduced onshore moisture transports into SA (Reason et al., 2000). For DJF (Figure 7b), the CAM5 simulations identify twin upper-level anticyclonic circulations, especially over the South Pacific. To the southeast of this anticyclonic circulation a series of high-pressure cells, related to a barotropic Rossby wave response to ENSO-diabatic forcing (Hoskins and Karoly, 1981), appear over Patagonia, the South Atlantic, and southern Indian Ocean. Figure 7b also identifies increased geopotential heights over equatorial Africa. Higher geopotential heights over equatorial Africa and the southeast Atlantic produce convergent wind anomalies over SA. This increase in upper-level convergence and reduced onshore moisture transports appears consistent with reduced SA rainfall in the stronger (on average) 1981–2016 versus the more moderate 1921-1980 El Niño's.

Figure 7c,d show OND differences in CAM5 circulation. Interestingly, the near-surface wind response appears dominated by an IOD-like wind response over the eastern Indian

Ocean. Note the increase in geopotential heights over the Indian Ocean and around the maritime continent. To the northeast of the maritime continent, the gradient in this height field appears to divert convergent upper winds from the Subtropical Westerly Jet (STWJ), reducing precipitation near 150°E, 20°N. At the same time, increasing upper-level heights over the Indian Ocean, and the lack of a significant change in winds there, are suggestive of a lack of a change in the Indian Ocean branch of the Walker Circulation. These results appear consistent with Liebmann et al.'s (2014) suggestion that EA OND rains were not decreasing because of the influence of the warming of the Indian Ocean. Here we find robust seasonal connections between recent EA OND droughts (Figure 2b,e,h) and large increases in OND WEP SST (Figure 3h), but no increases in the frequency of EA OND droughts (Figure 3b). Figure 7c,d may help explain these results, since we find fairly localized changes in Indo-Pacific circulation and little change in the Indian Ocean Walker Circulation.

Figure 7e,f show MAM differences in the CAM5 for warm WNP 1981–2016 and 1921–1980 events. The Pacific near-surface wind response is characterized by winds consistent with increased low pressure near 160°E, 30°N and increased precipitation near the central Indian Ocean, maritime continent and SPCZ. Low-level equatorial westerly and easterly tendencies over the central Indian and Pacific

oceans appear consistent with an intensification of the Walker Circulation. Figure 7e identifies a very strong decrease $(\sim -1.5Z)$ in equatorial precipitation near 170°W. Unlike the WEP/OND case (Figure 7d), the WNP/MAM upper-level changes (Figure 7f) indicate substantial differences over the eastern Pacific. While both the OND/WEP and MAM/WNP cases exhibit strong upper-level high pressure increases near 160°W 50°N/S, the MAM upper-level height field over the eastern Pacific is substantially lower, leading to a zonal height gradient near 150°E 10°S/N. Unlike OND/WEP, for the MAM/WNP case this zonal gradient redirects the strong easterly anomalies associated with the high pressure cells near 50°N/S towards the Equator, leading to strong upper-level convergence near the dateline. Thus, the upper-level Pacific component of the WNP pattern consists of three components: (a) a high-pressure response poleward of the extratropical increase in Pacific SST, (b) a cyclonic response to the southeast of the SST increase, and (c) a zonal west-to-east height gradient near 150°E/25°N. These factors, acting in combination, produce a La Niña-like response over the central and western Pacific Ocean. While the WNP is moderately correlated with Niño 3.4 SST (r = -0.61, 1988–2017), warm WNP SSTs appear to enhance La Niña impacts, as seen in 2017 and simulated in Funk and Hoell (2015). Acting alone, without enhancements by La Niña, Western V-like SST can reduce EA MAM rainfall.

Focusing on MAM circulation changes over the Indian Ocean basin, we find westerly low-level wind changes conducive to a reduction in onshore moisture transports into EA. Looking aloft, we also find an increase in upper-level easterly winds. It has recently been advanced (Liebmann *et al.*, 2014; 2017) that an increase in the strength of the Indian Ocean branch of the Walker Circulation might account for the relatively recent increased teleconnections between EA MAM rainfall and Pacific SST (Table 5). The increase in upper Figure 7f winds over the eastern Indian Ocean and EA would be consistent with this hypothesis.

3.9 | Analysing changes in diabatic forcing in the CAM5 and CESM1 LENS simulations

We next turn to an analysis of changes in diabatic forcing using CAM5 and CESM1 LENS simulations. We begin by defining teleconnected regions, as we did for SST, but using instead the 20-member ensemble CAM5 mean precipitation responses. As in Figure 2a–c, Figure 8a–c show CAM5 precipitation composites for each season's six recent driest seasons. As in Figure 2d–f, Figure 8d–f show correlations between 1997 and 2015 CAM5 precipitation and SA/EA rainfall over Africa. Based on these maps, we select forcing regions in the equatorial Pacific (DJF), WEP/eastern Indian Ocean (OND), and WNP (MAM). These regions are similar but not identical to the SST boxes, because precipitation responses are not exactly co-located with SST variations.

Having identified CAM5 forcing regions, we next present the CESM1 LENS precipitation for strong versus moderate Niño 3.4/WEP/WNP warm events. These events are based on the standardized SST ranges shown in Figure 3g-i, and correspond with the SST difference fields shown in Figure 6d-f. The 40 CESM1 LENS simulations are interrogated for 2000-2016 and samples of strong and moderate warming events identified based on SST. The difference between these samples does not represent climate change per se, but rather helps us evaluate differences between strong and moderate events in a stationary environment with a larger number of samples than provided by history (40 simulations \times 17 years = 680 samples). Averaging across a relatively short time period helps limit the non-stationary influence of climate change. Averaging across 40 independent simulations helps limit the influence of natural decadal variability. Since we can sample across 40 simulations from a similar time period, issues related to global warming or natural decadal variability will be mitigated.

Figure 8g presents the differential DJF precipitation response pattern for strong versus moderate warm Niño 3.4 events. The event criteria are based on the thresholds shown in Figure 3g; a strong event is greater +1.7Z.The CESM1 LENS simulations indicate a large difference (>0.8Z) in standardized precipitation in many regions. Large precipitation increases are identified over the eastern equatorial Pacific, the southwestern and southeastern United States, equatorial and eastern Africa, the Middle East and southwest Asia. Precipitation reductions are identified over the maritime continent, Central America, the Caribbean, northern South America, the southeast Atlantic and the western edge of southern Africa. In both the CAM5 and CESM1 LENS experiments a +0.8 °C increase in eastern equatorial SST (Figure 9a,d) translates into a substantial increase in the magnitude of the El Niño precipitation response (Figure 7a and 8g).

The precipitation response differences for OND strong and moderate warm WEP events (Figure 8h) appear much more localized, with significant precipitation responses limited to East Africa, central southwest Asia, the Indian Ocean basin, and the west and central equatorial Pacific. Again, this limited response seems quite similar to the changes in 1981–2016 *versus* 1921–1980 warm WEP events (Figure 7c). Stronger WEP warm events appear associated with an IOD-like precipitation dipole between East Africa and the eastern Indian/western Pacific Ocean regions.

Turning to precipitation response differences for MAM strong and moderate warm WEP events (Figure 8I) we find precipitation enhancements across the WNP, and over the northeast and southeast Indian Ocean/western Pacific. Precipitation is reduced over the equatorial Pacific from 140°E to 120°W. Precipitation reductions are also identified over East Africa, the Middle East, southwest Asia, and the southwestern United States. The CAM5 precipitation changes during 1981–2016 *versus* 1921–1980 warm WNP events (Figure 7e) look similar over the WNP and eastern Pacific, and the CAM5

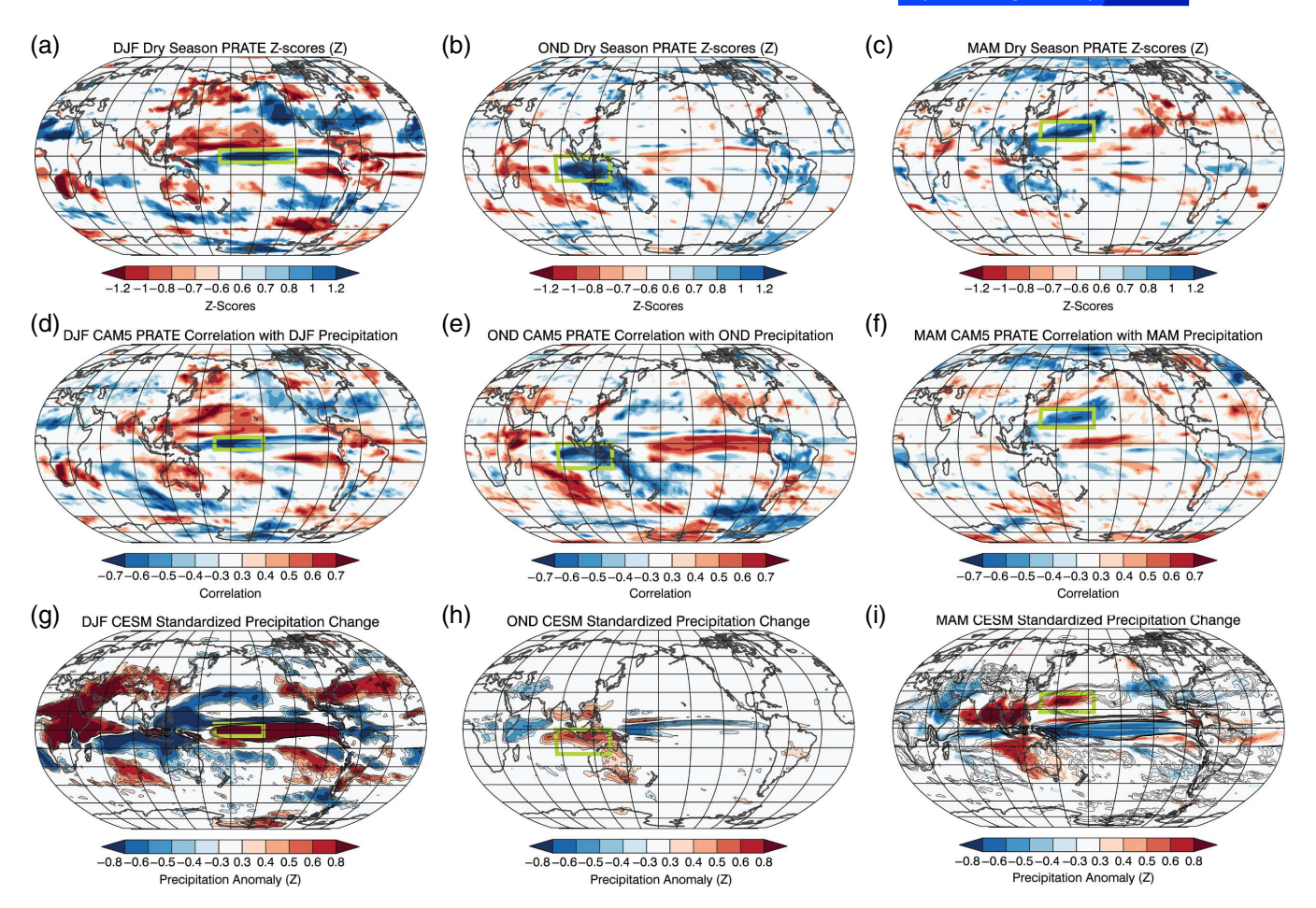


FIGURE 8 (a–c) Composites of standardized seasonal CAM5 ensemble average precipitation (PRATE) for the six driest seasons between 1981 and 2016. Values not significant at p < .1 have not been coloured. DJF dry seasons: 1991/1992, 1982/1983, 2015/2016, 1986/1987, 2001/2002 and 2002/2003. OND dry seasons: 2005, 1998, 1996, 1993, 2010 and 2016. MAM dry seasons: 2011, 1984, 2000, 2009, 1999 and 2004. (d–f). 1997–2016 CAM5 precipitation correlations with contemporaneous regional African rainfall. Values not significant at p < .1 have not been coloured. (g–i) Precipitation response for strong *versus* medium 2000–2016 warm events from the CESM1 LENS ensemble. Changes screened for significance at p < .1

simulations show a \sim -0.5Z reduction in rainfall across northeast East Africa and the Middle East. The pattern of precipitation increases over the eastern Indian Ocean/western Pacific looks quite different in the CAM5 and CESM1 LENS simulations, but both show an enhancement of precipitation consistent with EA drying. It is interesting to note that the drying features of the equatorial Atlantic/Congo Basin shown in the CAM5 simulations are absent from the CESM1 LENS simulated changes. These may be related to natural decadal variability, most likely within the observed Atlantic SST record.

We next turn to an analysis of CAM5 diabatic forcing (Figure 9a–c) within the regions identified in Figure 8a–f. Eastern Pacific SSTs have strong nonlinear relationships with east Pacific precipitation (Cai *et al.*, 2015a; 2015b), and this relationship is apparent in Figure 9a, which shows standardized CAM5 Niño 3.4 precipitation from 1921 to 2016. Observed strong El Niño's have SST corresponding to $\sim +2.2$ standardized anomalies. The corresponding CAM5 precipitation can be substantially greater, on the order of +3.2Z. This increase in diabatic forcing may be important, because both the equatorially trapped Matsuno–Gill Rossby–Kelvin wave

atmospheric responses (Gill, 1980) and off-equatorial Rossby wave responses (Hoskins and Karoly, 1981) are thought to scale with diabatic forcing.

Turning to 1921-2016 WEP OND CAM5 precipitation (Figure 9b), we note first the interesting discrepancy between the strong upward increase in WEP OND SST and the lack of an associated increase in OND WEP precipitation. The stationarity of the CAM5 WEP precipitation is consistent with the stationarity of the EA OND rainfall time series (Figure 3b). The CAM5 WEP precipitation time series and EA OND CHIRPS time series, however, both exhibit substantial interannual variation. The extreme 1997 OND EA rains were accompanied by a dramatic El Niño-related negative WEP rainfall anomaly. The following year (1998) was accompanied by warm WEP SST conditions, which was a La Niña-like climate state: increased WEP precipitation, a negative IOD state, and below-average EA rains. Following the 2008/2009 and 2015/2016 El Niño events, warm OND WEP SST were accompanied by increased WEP CAM5 precipitation and below normal CHIRPS EA OND precipitation. OND of 2016 also exhibited a negative IOD state and hence accounted for poor EA OND rainfall performance.

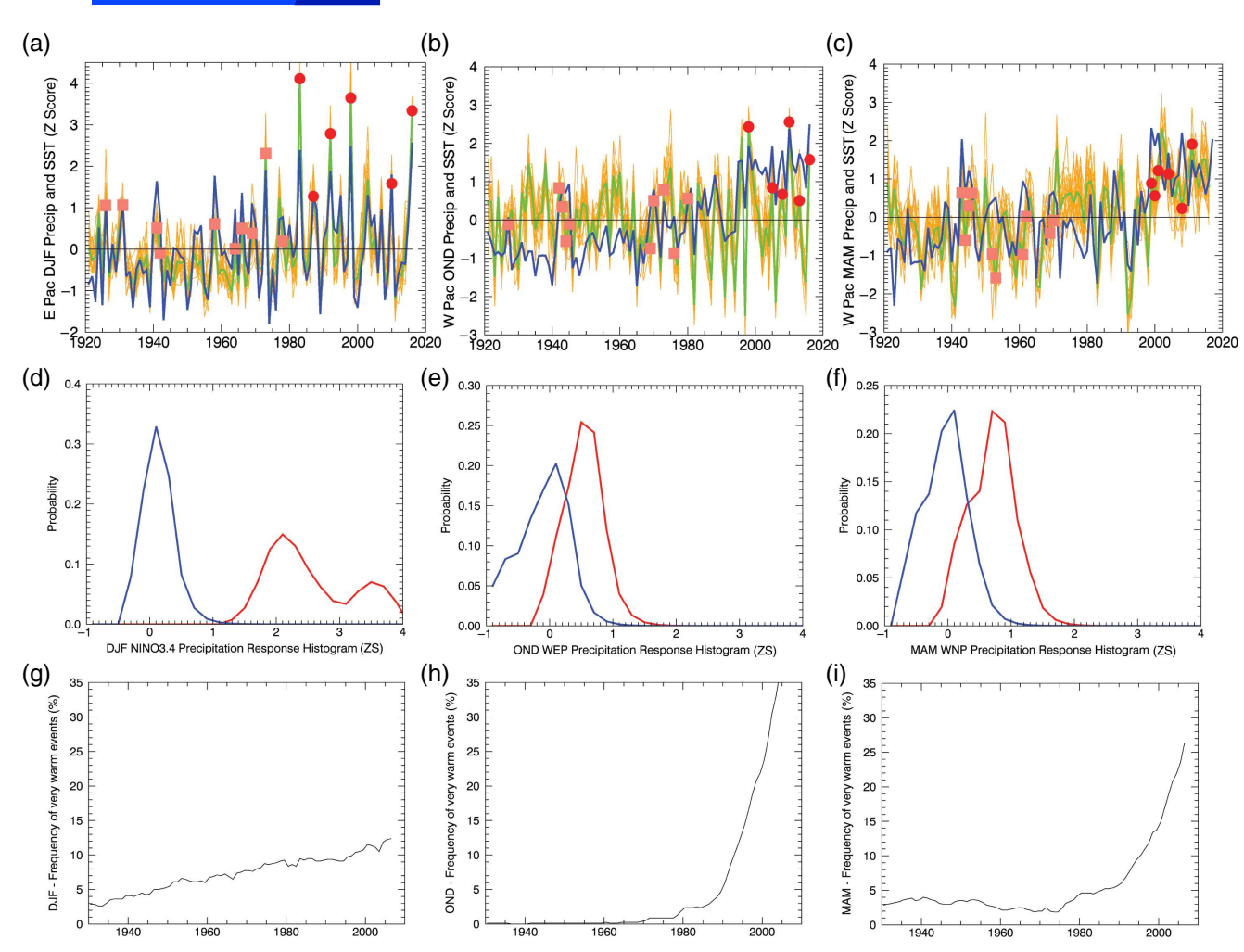


FIGURE 9 CAM5 and CESM1 diabatic forcing changes. (a–c) Standardized CAM5 precipitation from forcing regions defined in Figure 8. Based on a 1921–2016 baseline. Orange lines show individual simulations. The green line shows the ensemble average. The blue line corresponds to SST in either Niño 3.4 (DJF) or west Pacific (MAM, OND) for the regions shown in Figure 2. Orange squares and red circles identify the 1921–1980 and 1981–2016 1-in-6 year extremes from Figure 3. (d–f) PDFs of CESM1 LENS precipitation for moderate (blue) and very warm (red) events in the Niño 3.4, WEP and WNP regions. Based on standardized precipitation centred on a 1981–2010 baseline. (g–i) Frequency of very warm events, based on the CESM1 LENS for DJF Niño 3.4, OND WEP and MAM WNP

The CAM5 WNP MAM precipitation responses, on the other hand, indicate a strong step-like increase at the end of the twentieth century, consistent with the increase in WNP SST at this time (Figure 9c). Interestingly, CAM5 precipitation extrema during the mid-1940s, when the WEP region was quite warm (Figure 3i), were similar to the present extrema. This period was unique in that it was one of the longest stretches of consecutive dry MAM seasons on record for EA (four years in a row) (Figure 3c). Overall, changes between the 1921–1980 and 1981–2016 extrema are substantial, on the order of +0.7Z. The timing and magnitude of this change may be consistent with the decline in EA MAM rains (Figure 4).

We next present precipitation probability distribution functions (PDFs) for CESM1 LENS precipitation for strong and moderate 2000–2016 events (Figure 9d–f). These data have been centred on a 1981–2010 mean. Again, broadly consistent with the CAM5 simulation results, the CESM1 LENS simulations indicate large ($\sim +2Z$) increases in Niño 3.4 precipitation and moderate ($\sim +0.8Z$) increases in WEP and WNP.

3.10 | Assessing changes in warm event frequencies

We briefly assess warm event frequencies based on the 40 CESM1 LENS simulations (Figure 9g-i). These time series show the frequency with which the CESM1 LENS SST time series exceeded the thresholds defined in Figure 3g-i. Figure 9g indicates that the return period for a strong Niño 3.4 event has decreased from around 30 years to about 8 years (broadly consistent with the spacing of the 1982/1983, 1997/1998 and 2015/2016 events). Figure 9h,i show changes in CESM1 LENS WEP OND and WNP MAM frequencies - both exhibit dramatic increases in the twenty-first century, consistent with the multi-model analysis presented in Table 7. As discussed earlier, trends and interannual variability in SST in these regions would be influenced by anthropogenic warming and natural fluctuations associated with processes like ENSO and the IOD. Speaking to this point, Figure 10 shows a statistical reconstruction (regression estimate) of unsmoothed observed WNP SST (red line) based on, first, the WNP SST average from 53 multi-model climate

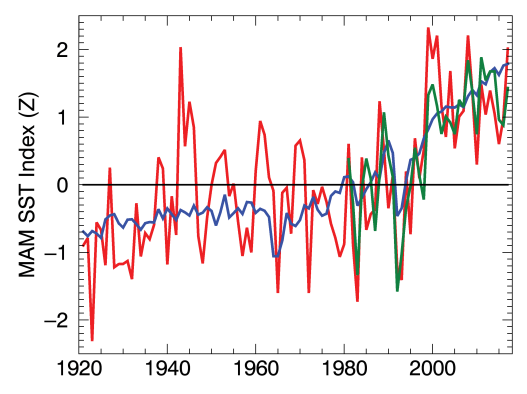


FIGURE 10 Observed seasonal WNP MAM SST (red) and a multi-model climate change estimate of WNP SST (blue). Also shown are estimates of 1981–2017 WNP SST based on a regression with the climate change ensemble average and observed Niño 3.4 SST (green). Extending the regression further back in time damped the 1998–2017 ENSO contributions to the WNP

change simulations (Table 3), and second, this climate change signal plus observed Niño 3.4 SST (green line). The climate change component explains 42% of the observed WNP variance. Together, the two components explain 72% of the observed 1981–2017 variability. Recent WNP variations can be largely explained as an interaction between climate change and ENSO, with the former and latter explaining 42 and 30% of the variability.

3.11 | Increased Niño 3.4 and Western V sea-surface temperatures

Figure 11a,b show, respectively, 1921–2017 and 1980–2017 time series of standardized monthly SST for the Niño 3.4 region and the "Western V" region, represented in this study by the average of WEP and WNP SST. Recent Indo-Pacific warming tendencies have tended to form a band of SST that originates near the maritime continent and stretches towards the northeast and southeastern extratropics (Lyon and DeWitt, 2012; Liebmann et al., 2014), and this structure has been referred to as the "Western V" (Funk and Hoell, 2015). This pattern, associated with the West Pacific Warming Mode, indicates a stronger Walker Circulation mechanism and enhanced subsidence across East Africa during MAM (Funk and Hoell, 2015) and DJFMAM (Funk and Hoell, 2017). Grey rectangles in Figure 11 delineate periods when Niño 3.4 SST exceeded +1.7Z followed by Western V SST values greater than +1.7Z. The Western V region shows a well-documented upward trend (Williams and Funk, 2011; Funk and Hoell, 2015), thought to increase the frequency of back-to-back OND and MAM droughts (Hoell and Funk, 2013a), and the SST gradients and impact associated with recent La Niña events (Williams and Funk, 2010; Hoell and Funk, 2013b; Hoell et al., 2014). What has not been discussed, in the context of African drought early warning, is the tendency for Western V SST to spike upward following El Niño events, such as that which occurred in the early

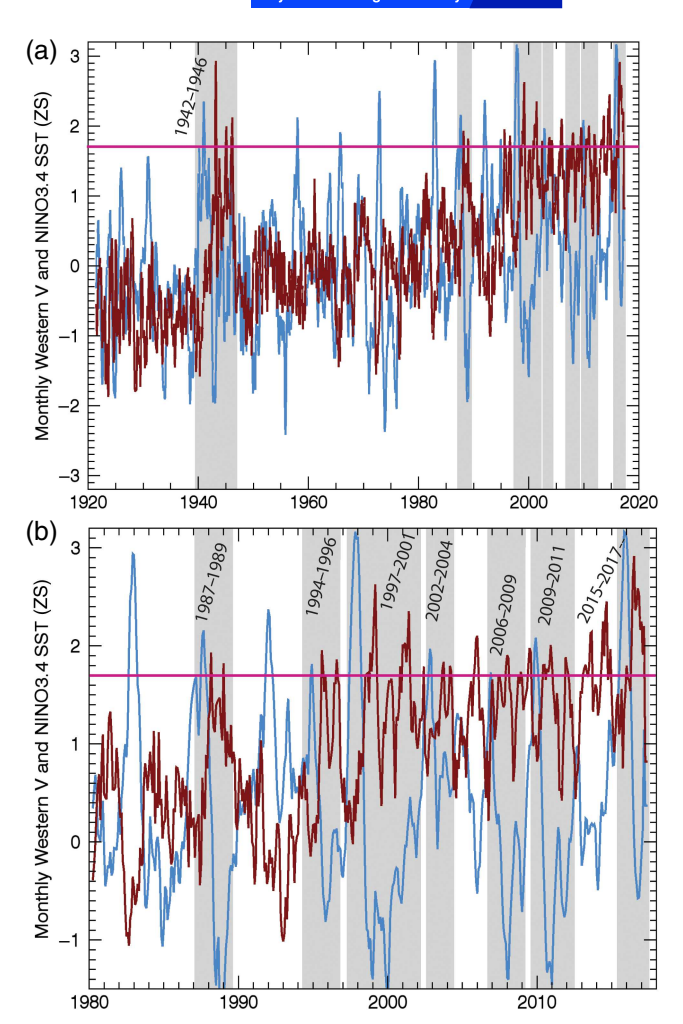


FIGURE 11 (a) 1921–2017 standardized monthly Niño 3.4 (blue) and Western V sea-surface temperature anomalies. (b) 1980–2017 standardized monthly Niño 3.4 and west Pacific sea-surface temperature anomalies

1940s. Figure 11a shows the strong 1942 El Niño followed by extreme and persistent warm Western V SST. Between 1921 and 1980 we identify one +1.7Z/+1.7Z Niño 3.4/Western V event (1942–1946). Between 1981 and 2017, we identify seven of these events. Between 1921 and 1980, four El Niño events exceeded +1.7Z; only the 1942–1946 era was associated with Western V SST greater than +1.7Z. Between 1981 and 2017, eight El Niño events had Niño 3.4 SST greater than +1.7Z. Of these eight events, six were followed by Western V SST greater than +1.7Z.

3.12 | Tendency for Western V SST to spike upward following El Niño events

Looking in more depth at the recent (1980–2017) era (Figure 11b, note that Figure 11b is just an expanded version of Figure 11a), we find that the 1987/1988 El Niño was followed by +1.3 to +1.8Z Western V SST concurrent with ~ -1.5 Z Niño 3.4 SST in 1988/1989. Then the +1.8Z 1994/1995 Niño 3.4 conditions were followed by cold -0.8Z (warm +1.8Z) Niño 3.4 (Western V) SST. After the very warm (+3.1Z) 1997/1998 event we find a step-like increase

in Western V SST. This increase is probably associated with the recent decline in East African rains (Lyon and DeWitt, 2012; Funk *et al.*, 2014). Here, however, we are interested in the seasonal covariations of the ENSO and Western V SST, which may act together to produce multi-year climate anomalies like the extreme 1997/1998 El Niño and the La Niña-like 1999–2001 "Perfect Ocean for Drought" that followed (Hoerling and Kumar, 2003).

3.13 | How recent back-to-back ENSO plus Western V have related to recent droughts

After 2001 we find oscillations producing poor SA and EA food security outcomes. The moderate 2006/2007 El Niño event, associated with poor SA rainfall and crop production, was followed by 2007/2008 La Niña conditions accompanied by warm Western V SST: OND of 2007 and MAM of 2008 EA rains were poor, and by boreal spring of 2008, EA faced a severe food crisis. Warm Western Pacific SST are consistent with La Niña conditions; the 2007–2008 ~ +1.7Z Western V SST likely exhibit both influences from both La Niña conditions and influence from anthropogenic warming (Funk and Hoell, 2015). Contemporaneous Niño 3.4 SST values were cool, with standardized anomalies of less than –1Z.

In 2009/2010 an El Niño occurred, and Zimbabwe and Mozambique rainfall was poor. The following OND 2010 and MAM 2011 were associated with cool (-1.2Z) Niño 3.4 and warm (+1.8Z) Western V SST, and severe droughts over eastern Africa. Despite advance warning (Hillbruner and Moloney, 2012), more than 260,000 Somali lives were lost as a result of these back-to-back droughts, political turmoil, and civil conflict (Checchi and Robinson, 2013).

In 2015/2016, a strong El Niño formed, and Western V SST reached the highest values in the historic record (~ +2.9 standardized anomalies). Despite moderate ENSO and IOD conditions (Table 4), back-to-back OND/MAM droughts contributed to poor harvests and pasture conditions, and food aid was required for more than 30 million people in 2017 (Table 1).

The data displayed in Figure 11 indicate (a) an oscillatory pattern between warm eastern and western Pacific SST conditions, (b) a propensity for an increase in the number of El Niño's with Niño 3.4 SST greater than +1.7Z, and (c) an upward trend in western Pacific SST. A high-frequency jump in western Pacific SST often follows strong (+1.7Z) El Niño's. This occurred 75% of the time (six out of eight events) since 1981. While these results are suggestive, ENSO is inherently very variable, and it is possible to find large multi-year increases and decreases in ENSO strength in long pre-industrial climate simulations without any change in external forcing (Wittenberg, 2009). This leads to the question: "Is the oscillatory warming behaviour found in observed SST a common pattern in the current generation of climate change models?"

3.14 | Is oscillatory warming behaviour found in observed SST a common pattern in the current generation of climate change models?

To explore this question, we plot 16 Hovmüller (time versus longitude) diagrams (Figure 12), showing standardized 1921–2016 monthly equatorial (10°S–10°N) Indo-Pacific (70°E–90°W) SST from the observed ERv4 dataset (far left), 14 individual simulations from 14 different models (Table 3), and the average of the standardized climate change simulations (far right). Each longitude section is standardized based on the 1921-2016 time period. Our goal with this figure is to suggest visually that most of the models appear to produce ENSO variations and increases in SST that are quite similar to the observations. Note that since each climate simulation produces its own independent set of ENSO events, any similarities in timing across the simulations or observations are accidental. Within the observed record (Obs column) we see infrequent but increasingly warm east Pacific SST in the latter part of the record, a stronger systematic warming trend in the western Pacific, and several occurrences in which a strong east Pacific warm event is followed by western Pacific warming. Table 8 quantifies these tendencies for all 54 members of our fully-coupled climate change ensemble (Table 3), using equatorial (10°S–10°N) DJF Niño 3.4 and western Pacific (120-160°E) SST from the OND and MAM seasons. Contrasting 1981-2016 and the 1920-1980 time periods, these simulations indicate that the return time for a +1.7Z Niño 3.4 event changes from once every 40 years to once every 10 years. The western Pacific time series are strongly influenced by radiative forcing, and we find only one +1.6Z OND and MAM event in the 1921–1980 era. In the 1981–2016 era, +1.7Z events occur about once every 5 or 6 years, and when a +1.7Z Niño 3.4 event occurs, there is a \sim 37-40% chance that it is followed by a +1.7Z warm event. These results might indicate that early warning systems should be prepared for these types of climate variations - variations similar to the 1998-2001, 2009-2011 and 2015–2017 sequences.

Note that each of the individual Hovmüller diagrams (columns) is quite different from the ensemble average (far right). Insofar as droughts are driven by extremes in Indo-Pacific SST, as opposed to low-frequency trends in SST, the behaviour of the individual simulations may be more informative than the ensemble average. Several nonlinearities in the tropical Indo-Pacific climate system support this perspective. There are well-documented local nonlinearities relating very warm (>28 °C) tropical SST and precipitation. Above 26 °C there tends to be a steep increase in rainfall rates with increasing surface temperatures (Folkins and Braun, 2003), which is primarily due to increases in columnar water vapour (Neelin *et al.*, 2009). For east Pacific precipitation during El Niño's, there is a strong nonlinear relationship

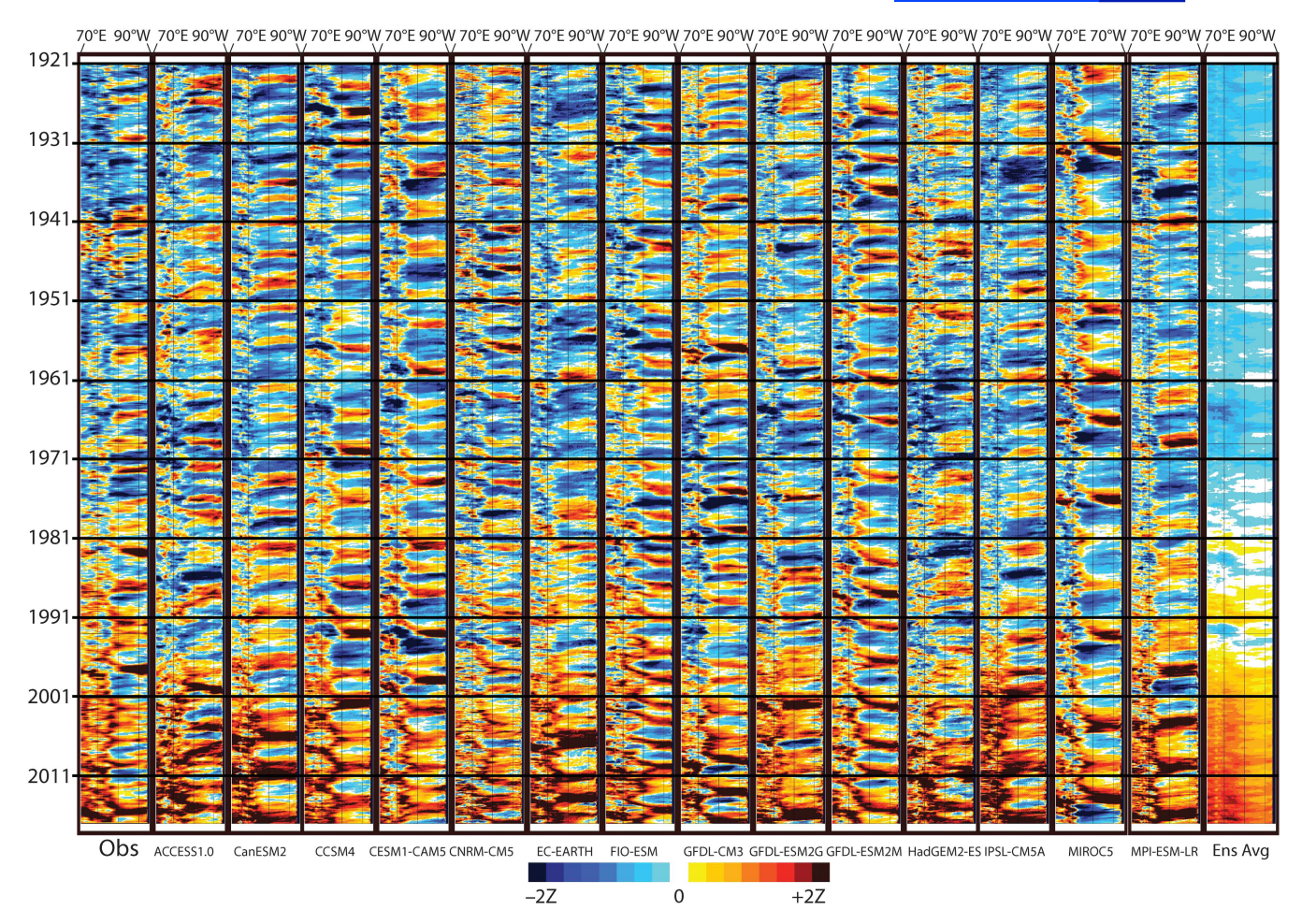


FIGURE 12 Howmüller plots of standardized monthly SST anomalies. Each panel depicts equatorial SST from either observations, a single model simulation, or the ensemble average. Panels begin at 70°E and end at 90°W

 TABLE 8
 Analysis of CMIP5 climate change simulations.

	DJF Niño 3.4 > +1.7Z	OND WP>+1.7Z	MAM WP>+1.7Z	DJF N34 & OND WP > +1.7Z	DJF N34 & OND WP > +1.7Z
1921-1980 counts	79	1	1	1	1
1981-2016 counts	196	315	351	69	75
1921-1980 percent	2.5%	0.0%	0.0	0.0	0.0
1981-2016 percent	10.1%	17%	19%	37%	40%

between east Pacific precipitation, SST, and meridional temperature gradients (Cai *et al.*, 2014; 2015b). These precipitation responses contribute directly to the diabatic forcing (Gill, 1980) that helps maintain the anomalous El Niño circulation, trade wind reduction, and decreased equatorial upwelling. At the demise of El Niño, normal trade wind patterns re-establish themselves, piling up warm waters in the western Pacific.

4 | DISCUSSION

The results presented in Figure 9g need to be interpreted carefully on a case-by-case basis. Figure 9g indicates that the return period for a strong Niño 3.4 event has decreased from around 30 years to about 8 years (broadly consistent with the spacing of the 1982/1983, 1997/1998 and 2015/2016 events).

Given the coherent and large CAM5 and CESM1 LENS difference results presented here, an increased frequency of these events would likely be accompanied by more extreme El Niño climate disruptions, consistent perhaps with the observed impacts of strong El Niño's on SA (Hoell *et al.*, 2015). It is also possible, as discussed above, that these strong El Niño's might be followed by warm WEP and WNP conditions and increases in the risk of drought in EA.

While the future state of ENSO is still poorly understood and uncertain (Christensen *et al.*, 2013), there is some increasing consensus that strong El Niño's are becoming more frequent. While Guilyardi *et al.* (2012) find that the balance of feedbacks in different models can lead to different changes in ENSO characteristics, Kim *et al.* (2014) screen models based on their ability to capture these feedbacks, and find a robust increase in ENSO variability up to

2040 – suggesting that part of the uncertainty in previous assessments was associated with divergent late twenty-first century changes in amplitude. Cai *et al.* (2015a) provide a review of ENSO climate change research suggesting that "accelerated equatorial Pacific warming, especially in the east, is expected to induce extreme rainfall in the eastern equatorial Pacific ENSO-related catastrophic weather events are thus likely to occur more frequently with unabated greenhouse gas emissions". This study also finds that "Long records of paleo-ENSO variance suggest that twentieth century ENSO activity was stronger than that during previous centuries (Li *et al.*, 2013; McGregor *et al.*, 2013) and millennia (Cobb *et al.*, 2003)."

Without making any assertions about trends in ENSO-like climate (i.e. whether the mean future climate will look more El Niño-like or La Niña-like), the observational evidence examined here (Figures 3g and 9a), a multi-model suite of climate change simulations (Table 7), and the CESM1 LENS ensemble (Figure 9g), all suggest that strong El Niño's are becoming more frequent. The CAM5 and CESM1 LENS simulations analysed here help confirm Cai *et al.*'s (2015b) assertion that very warm east Pacific SSTs appear alongside increases in deep convection that trigger a quasi-global reorganization of tropical circulation, helping to explain stronger negative impacts on SA DJF rainfall (Figure 3d and Hoell *et al.*, (2015)).

Unusually warm OND WEP SSTs also appear to have a negative impact on EA OND rains, but only on seasonal as opposed to decadal time-scales. Given EA's food security concerns, it is interesting to note three extreme WEP diabatic forcing and SST (Figure 9b) events occurred in 1999, 2010 and 2016, following the 1997/1998, 2008/2009 and 2015/2016 El Niño's. These years were also negative IOD seasons. Research has suggested that the deleterious influence of western Pacific SST on both short and long rains (Hoell and Funk, 2013a) may help explain the co-occurrence of back-to-back short and long rainy season droughts. The results presented here indicate little change in the OND Walker Circulation (Figure 9b), so the rapid increase in observed WEP SST (Figure 3h) or CESM1 LENS WEP frequencies (Figure 9h) does not seem to be translating into more frequent EA OND droughts. When these droughts occur, however, they may tend to be in phase with MAM droughts, and follow El Niño events (Figure 2). For fragile pastoral and agro-pastoral communities, back-to-back droughts are particularly damaging.

Unusually warm MAM WNP SSTs appear to have a negative impact on EA MAM rains on both seasonal and decadal time-scales. While some research has asserted that MAM rains have a weak association with Indo-Pacific SST, and low-frequency variability dominated by natural decadal variability (Lyon, 2014; Yang *et al.*, 2014), we find strong connections between EA MAM rainfall and WNP SST at both the seasonal (Figure 3f) and decadal time-scales (Figure 4). WNP SST variations, in turn, appear largely driven

by external radiative forcing and ENSO. Figure 10 shows unsmoothed observed WNP SST and the WNP average from 53 multi-model climate change simulations (Table 3). This ensemble explains 42% of the observed WNP variance. Combining this with observed Niño 3.4 SST (green line) explains 72% of the 1981–2017 variability. Recent WNP variations can be largely explained as an interaction between climate change and ENSO.

One striking aspect of the observed MAM time series (Figure 3c) is the large decrease in the number of wet EA MAM events. Analysis of sub-seasonal (pentadal) MAM CHIRPS and SST data (Vigaud et al., 2017) identify a cool Western V-like SST structure and warm eastern equatorial Pacific SST as conducive to robust EA rains. This analysis produced results that appear quite similar to Figure 2c. Increases in WNP SST (Figure 10) and WNP precipitation extrema (Figure 9c) appear likely to have increased and decreased the frequency of East African droughts and pluvials. This view is consistent with prior research emphasizing the interaction of La Niña with the Western Pacific Gradient (Hoell et al., 2013; 2014; Hoell and Funk, 2013b), but places more emphasis on the WNP region, consistent with research stressing the important role of these extratropical SSTs (Lyon and DeWitt, 2012; Lyon et al., 2013; Lyon, 2014; Yang et al., 2014).

While the limited historic record makes analysis difficult, we have suggested that for the purposes of African drought monitoring and prediction, a "quasi-oscillatory" view of climate change may help understand and anticipate extremes. Relief agencies should be prepared for a world in which SSTs in any given year look more like a single simulation, rather than multi-model ensemble average response of SST. SST within such a realization will be primarily due to natural variability, influenced by climate change. Indo-Pacific SST will likely continue to behave like individual climate change simulations, or the observed historical record, which appear to favour more extreme east Pacific warm events, often followed by La Niña-like cool conditions combined with increases in WEP and WNP SST. In the quasi-oscillatory view, more heat is added to the system, but it moves around, with ENSO being a primary driver of these movements. Warm waters pile up in the western Pacific, and then westerly wind bursts trigger El Niño's. When these events happen, the CESM1 LENS simulations suggest that we may be likely to see stronger SST gradients and precipitation responses, which could happen in sequences like those experienced when 1997/1998, 2006/2007, 2009/2010 and 2015/2016 El Niño's were followed by warm WEP/WNP SST and dry EA conditions. While more research into these variations will be necessary, understanding such sequencing may help relief agencies build contingency plans addressing the possibility of increased periods of drought.

Whatever the cause or temporal sequence, this study has supported prior research indicating that the magnitude of Niño 3.4, WEP and WNP SST anomalies matter, with strong

RMetS

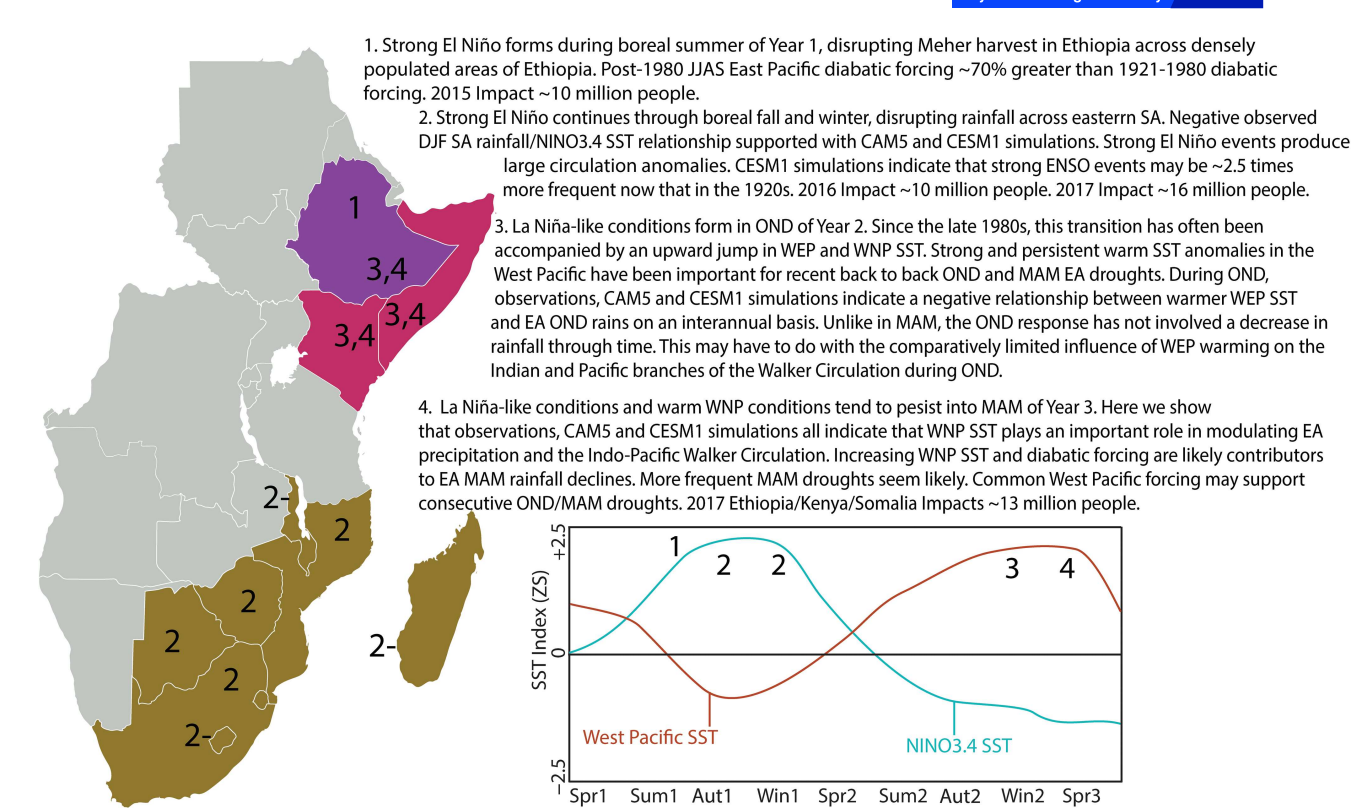


FIGURE 13 Schema describing sequential SA/EA drought sequence and associated opportunities for prediction

warm events associated with larger changes in diabatic forcing and circulation. Such SST patterns may provide targets of opportunity for more effective seasonal prediction.

5 | CONCLUSION

Figure 13 summarizes the potential opportunities for prediction discussed in this study. Extremes in Indo-Pacific SST are accompanied by extremes in equatorial diabatic forcing (Funk *et al.*, 2016a; 2016b), as shown in Figure 9. These extremes trigger atmospheric Rossby wave responses (Gill, 1980; Hoskins and Karoly, 1981) enhancing drought frequencies over northern Ethiopia (Korecha and Barnston, 2007; Korecha and Sorteberg, 2013) and SA (Jury *et al.*, 1994; Nicholson, 1997; Nicholson and Kim, 1997; Reason *et al.*, 2000; Misra, 2003; Ratnam *et al.*, 2014; Hoell *et al.*, 2015; 2017a). Recent warm ENSO events have been warmer (Table 6) and more energetic (Figure 9a). CAM5 and CESM1 DJF simulations support observational analyses (Ratnam *et al.*, 2014; Hoell *et al.*, 2015) indicating that unusually warm El Niño's are often associated with SA drought.

Since 1981, six out of eight strong (>+1.7Z Niño 3.4 SST) El Niño events have been followed by strong (>+1.7Z) Western V SST. The associated WEP and WNP SST extrema appear to be effective indicators of EA OND and MAM droughts. In the 20 years of data identified in Figure 3e,f, four strong (>+1.7Z Niño 3.4 SST) El Niño events occurred, and three of these events (1997/1998, 2009/2010 and 2015/2016) were followed by consecutive OND/MAM droughts in

1998/1999, 2010/2011 and 2015/2016. Further observational and modelling analysis supporting the understanding and prediction of these extremes may enhance our ability to anticipate and mitigate back-to-back EA droughts. Climate change may be increasing the frequency of these unusually warm events (Table 8, Figure 9g–i), and the strong anthropogenic WNP warming (Figure 10) appears to be associated with significant enhancements of the Walker Circulation (Figure 7e and 8i) and potentially predictable EA MAM droughts (Figure 3f).

In the context of seasonal prediction efforts, such as those carried out by the regional Climate Outlook Forum communities for Eastern and Southern Africa, this work my indicate that traditional ENSO-dependent monitoring and forecasting efforts could be enhanced using additional indices like WEP and WNP. While warm SSTs in these regions create La Niña-like modulations in the Indo-Pacific Walker Circulation, they explain substantially more EA OND/MAM variance. This result is especially important for EA MAM rains, which are generally considered difficult to predict. The WNP indicator correctly identifies all of the recent droughts (Figure 3f), and the extensive analysis of CAM5 and CESM1 simulations explored here provide a cogent physical explanation for this statistical relationship.

In the context of climate change research, such as that discussed in the Intergovernmental Panel on Climate Change Assessment Reports, this work advances our understanding in two ways. First, we suggest that "climate change" may manifest as a shift in the intensity of SST extremes, as well as shifts in long-term means. Dynamic feedbacks redistribute

the increasing heat in the ocean, so that as the ocean warms we may experience both more intense El Niño warm events (Figure 6d) and more intense WNP warm events (Figure 6f); with the equatorial trade winds modulating Ekman pumping and the Bjerknes feedback to warm and cool the equatorial Pacific, creating enhanced gradients and Walker Circulation modulations. Identifying and predicting these extremes will provide one means of adaptation for eastern and southern Africa. Second, working from the observed EA MAM dry events and SST correlation structure, this work has supported a line of research linking anthropogenic warming with EA MAM rainfall declines (Verdin et al., 2005; Williams and Funk, 2011; Funk et al., 2014; Funk and Hoell, 2015; 2017), but with results consistent with studies emphasizing the important role played by the extratropical North Pacific (Lyon and DeWitt, 2012; Lyon, 2014; Yang et al., 2014; Vigaud et al., 2017). The "East Africa climate paradox" (Rowell et al., 2015) might be resolved by considering that (a) WNP SST is strongly influenced by climate change (Figure 10), and (b) WNP SST strongly influences EA MAM rainfall (Figure 2 and 3c) and the Walker circulation (Figures 5 and 7), but (c) climate change models struggle to correctly represent EA MAM rainfall (Yang et al., 2014; Tierney et al., 2015), and may be overestimating the ENSO-related warming signal (Funk and Hoell, 2015).

ACKNOWLEDGEMENTS

This work was primarily supported by USGS cooperative agreement No. G14AC00042 and NASA grant No. NNX16AM02G. Chris Funk is supported under the USGS Drivers of Drought programme. Catherine Pomoposi is supported by the Postdocs Applying Climate Expertise (PACE) programme.

Conflict of interest

The authors confirm that they have no conflicts of interest pertaining to this manuscript or the research it describes.

ORCID

Chris Funk http://orcid.org/0000-0002-9254-6718

REFERENCES

- Becker, A., Finger, P., Meyer-Christoffer, A., Rudolf, B., Schamm, K., Schneider, U. and Ziese, M. (2013) A description of the global land-surface precipitation data products of the Global Precipitation Climatology Centre with sample applications including centennial (trend) analysis from 1901-present. Earth System Science Data, 5, 71–99.
- Behera, S., Salvekar, P. and Yamagata, T. (2000) Simulation of interannual SST variability in the tropical Indian Ocean. *Journal of Climate*, 13, 3487–3499.
- Behera, S.K., Luo, J.-J., Masson, S., Delecluse, P., Gualdi, S., Navarra, A. and Yamagata, T. (2005) Paramount impact of the Indian Ocean dipole on the East African short rains: a CGCM study. *Journal of Climate*, 18, 4514–4530.
- Behera, S.K. and Yamagata, T. (2001) Subtropical SST dipole events in the southern Indian Ocean. *Geophysical Research Letters*, 28, 327–330.

- Bowden, J.H. and Semazzi, F.H. (2007) Empirical analysis of intraseasonal climate variability over the Greater Horn of Africa. *Journal of Climate*, 20, 5715–5731.
- Bretherton, C.S. and Park, S. (2009) A new moist turbulence parameterization in the Community Atmosphere Model. *Journal of Climate*, 22, 3422–3448.
- Cai, W., Borlace, S., Lengaigne, M., van Rensch, P., Collins, M., Vecchi, G., Timmermann, A., Santoso, A., McPhaden, M.J., Wu, L., England, M.H., Wang, G., Guilyardi, E. and Jin, F.-F. (2014) Increasing frequency of extreme El Niño events due to greenhouse warming. *Nature Climate Change*, 4, 111–116.
- Cai, W., Santoso, A., Wang, G., Yeh, S.-W., An, S.-I., Cobb, K.M., Collins, M., Guilyardi, E., Jin, F.-F., Kug, J.-S., Lengaigne, M., McPhaden, M.J., Takahashi, K., Timmermann, A., Vecchi, G., Watanabe, M. and Wu, L. (2015a) ENSO and greenhouse warming. *Nature Climate Change*, 5, 849–859.
- Cai, W., Wang, G., Santoso, A., McPhaden, M.J., Wu, L., Jin, F.-F., Timmermann, A., Collins, M., Vecchi, G., Lengaigne, M., England, M.H., Dommenget, D., Takahashi, K. and Guilyardi, E. (2015b) Increased frequency of extreme La Niña events under greenhouse warming. *Nature Climate Change*, 5, 132–137.
- Checchi, F. and Robinson, W.C. (2013) Mortality Among Populations of Southern and Central Somalia Affected by Severe Food Insecurity and Famine During 2010–2012. Rome: Food and Agriculture Organization of the United Nations.
- Christensen, J.H., Kanikicharla, K.K., Marshall, G. and Turner, J. (2013) Climate phenomena and their relevance for future regional climate change. In: Stocker, T.F., Qin, D., Plattner, G.-K., Tignor, M.M.B., Allen, S.K., Boschung, J., Nauels, A., Xia, Y., Bex, V. and Midgley, P.M. (Eds.) Climate Change 2013: The Physical Science Basis. Contribution of Working Group I to the Fifth Assessment of the Intergovernmental Panel on Climate Change. Cambridge: Cambridge University Press, pp. 1217–1308.
- Clark, C.O., Webster, P.J. and Cole, J.E. (2003) Interdecadal variability of the relationship between the Indian Ocean zonal mode and East African coastal rainfall anomalies. *Journal of Climate*, 16, 548–554.
- Cobb, K.M., Charles, C.D., Cheng, H. and Edwards, R.L. (2003) El Niño/Southern Oscillation and tropical Pacific climate during the last millennium. *Nature*, 424, 271–276.
- FEWSNET. (2017a) Decreases in staple food prices likely due to humanitarian assistance.
- FEWSNET. (2017b) Already unprecedented food assistance needs grow further; risk of Famine persists. Available at: http://www.fews.net/sites/default/files/FEWS%20NET%20Global%20FS%20Alert_20170621.pdf.
- Folkins, I. and Braun, C. (2003) Tropical rainfall and boundary layer moist entropy. *Journal of Climate*, 16, 1807–1820.
- Frankenberger, T.R. and Verduijn, R. (2011) Integrated Food Security Phase Classification (IPC). http://www.ipcinfo.org/fileadmin/user_upload/ipcinfo/docs/1_IPC_Glob_Proj_Eval_04_11_Report.pdf
- Funk, C. (2016) Concerns about the Kenya/Somalia short rains. Available at: http://blog.chg.ucsb.edu/?m=201610 [Accessed October 2016].
- Funk, C., Davenport, F., Harrison, T.M., Gideon Galu, L., Pomposi, C., Macharia, D., Husak, G.J., and Faka, D. (2018) Anthropogenic enhancement of moderate-to-strong El Niño events likely contributed to drought and poor harvests in Southern Africa during 2016. Bulletin of the American Meteorological Society, 99, S91–S96.
- Funk, C., Dettinger, M.D., Michaelsen, J.C., Verdin, J.P., Brown, M.E., Barlow, M. and Hoell, A. (2008) Warming of the Indian Ocean threatens eastern and southern African food security but could be mitigated by agricultural development. Proceedings of the National Academy of Sciences of the United States of America, 105, 11081–11086.
- Funk, C., Harrison, L., Shukla, S., Korecha, D., Magadzire, T., Husak, G., Galu, G. and Hoell, A. (2016a) Assessing the contributions of local and east Pacific warming to the 2015 droughts in Ethiopia and Southern Africa. *Bulletin of the American Meteorological Society*, 97, S75–S80.
- Funk, C., Husak, G., Korecha, D., Galu, G. and Shukla, S. (2016b) Below normal forecast for the 2017 East African long rains. Available at: http://blog.chg. ucsb.edu/?m=201612 [Accessed December 2016].
- Funk, C. and Hoell, A. (2015) The leading mode of observed and CMIP5 ENSO-residual sea surface temperatures and associated changes in Indo-Pacific climate. *Journal of Climate*, 28, 4309–4329.
- Funk, C. and Hoell, A. (2017) Recent climate extremes associated with the West Pacific warming mode. In: Wang, S.-Y.S., Yoon, J.-H., Funk, C.C. and Gillies, R. (Eds.) Climate Extremes: Patterns and Mechanisms. Hoboken, NJ: Wiley Press, pp. 165–176.
- Funk, C., Hoell, A., Shukla, S., Bladé, I., Liebmann, B., Roberts, J.B. and Husak, G. (2014) Predicting East African spring droughts using Pacific and Indian

the RMetS

- Ocean sea surface temperature indices. *Hydrology and Earth System Sciences Discussions*, 11, 3111–3136.
- Funk, C., Nicholson, S.E., Landsfeld, M., Klotter, D., Peterson, P. and Harrison, L. (2015a) The centennial trends Greater Horn of Africa precipitation dataset. *Scientific Data*. 2, 150050.
- Funk, C., Peterson, P., Landsfeld, M., Pedreros, D., Verdin, J., Shukla, S., Husak, G., Rowland, J., Harrison, L., Hoell, A. and Michaelsen, J. (2015b) The climate hazards infrared precipitation with stations a new environmental record for monitoring extremes. *Scientific Data*, 2, 150066.
- Funk, C., Senay, G., Asfaw, A., Verdin, J., Rowland, J., Korecha, D., Eilerts, G., Michaelsen, J., Amer, S. and Choularton, R. (2005) Recent drought tendencies in Ethiopia and equatorial-subtropical eastern Africa. In: FEWS NET (Ed.) Vulnerability to Food Insecurity: Factor Identification and Characterization Report. Washington, DC: US Agency for International Development, p. 12.
- Gill, A.E. (1980) Some simple solutions for heat-induced tropical circulation. Quarterly Journal of the Royal Meteorological Society, 106, 447–462.
- Goddard, L. and Graham, N.E. (1999) Importance of the Indian Ocean for simulating rainfall anomalies over eastern and southern Africa. *Journal of Geophysical Research*, 104, 19099–19116.
- Guilyardi, E., Bellenger, H., Collins, M., Ferrett, S., Cai, W. and Wittenberg, A. (2012) A first look at ENSO in CMIP5. Clivar Exchanges, 17, 29–32.
- Hastenrath, S., Polzin, D. and Mutai, C.C. (2007) Diagnosing the 2005 drought in equatorial East Africa. *Journal of Climate*, 20, 4628–4637.
- Hillbruner, C. and Moloney, G. (2012) When early warning is not enough lessons learned from the 2011 Somalia famine. *Global Food Security*, 1, 20–28.
- Hoell, A. and Funk, C. (2013a) Indo-Pacific sea surface temperature influences on failed consecutive rainy seasons over eastern Africa. *Climate Dynamics*, 43, 1645–1660.
- Hoell, A. and Funk, C. (2013b) The ENSO-related west Pacific sea surface temperature gradient. *Journal of Climate*, 26, 9545–9562.
- Hoell, A., Funk, C. and Barlow, M. (2013) The regional forcing of Northern Hemisphere drought during recent warm tropical west Pacific Ocean La Niña events. *Climate Dynamics*, 42, 3289–3311.
- Hoell, A., Funk, C. and Barlow, M. (2014) La Niña diversity and the forcing of northwest Indian Ocean rim teleconnections. *Climate Dynamics*, 42, 3289–3311.
- Hoell, A., Funk, C., Magadzire, T., Zinke, J. and Husak, G. (2015) El Niño–Southern Oscillation diversity and Southern Africa teleconnections during austral summer. Climate Dynamics, 45, 1583–1599.
- Hoell, A., Funk, C., Zinke, J. and Harrison, L. (2017a) Modulation of the Southern Africa precipitation response to the El Niño Southern Oscillation by the subtropical Indian Ocean dipole. *Climate Dynamics*, 48, 2529–2540.
- Hoell, A., Hoerling, M., Eischeid, J., Quan, X.-W. and Liebmann, B. (2017b) Reconciling theories for human and natural attribution of recent East Africa drying. *Journal of Climate*, 30, 1939–1957.
- Hoerling, M. and Kumar, A. (2003) The Perfect Ocean for drought. Science, 299, 691–694
- Hoskins, B.J. and Karoly, D.J. (1981) The steady linear response of a spherical atmosphere to thermal and orographic forcing. *Journal of the Atmospheric Sciences*, 38, 1179–1196.
- Huang, B., Banzon, V.F., Freeman, E., Lawrimore, J., Liu, W., Peterson, T.C., Smith, T.M., Thorne, P.W., Woodruff, S.D. and Zhang, H. (2015) Extended reconstructed sea surface temperature version 4 (ERSST. v4). Part I: upgrades and intercomparisons. *Journal of Climate*, 28, 911–930.
- Husak, G.J., Michaelsen, J. and Funk, C. (2007) Use of the gamma distribution to represent monthly rainfall in Africa for drought monitoring applications. *International Journal of Climatology*, 27, 935–944.
- Indeje, M., Semazzi, F.H. and Ogallo, L.J. (2000) ENSO signals in East African rainfall seasons. *International Journal of Climatology*, 20, 19–46.
- Jury, M., McQueen, C. and Levey, K. (1994) SOI and QBO signals in the African region. *Theoretical and Applied Climatology*, 50, 103–115.
- Kay, J., Deser, C., Phillips, A., Mai, A., Hannay, C., Strand, G., Arblaster, J.M., Bates, S.C., Danabasoglu, G., Edwards, J., Holland, M., Kushner, P., Lamarque, J.-F., Lawrence, D., Lindsay, K., Middleton, A., Munoz, E., Neale, R., Oleson, K., Polvani, L. and Vertenstein, M. (2015) The Community Earth System Model (CESM) large ensemble project: a community resource for studying climate change in the presence of internal climate variability. *Bulletin* of the American Meteorological Society, 96, 1333–1349.
- Kim, S.T., Cai, W., Jin, F.-F., Santoso, A., Wu, L., Guilyardi, E. and An, S.-I. (2014) Response of El Niño sea surface temperature variability to greenhouse warming. *Nature Climate Change*, 4, 786–790.

- Korecha, D. and Barnston, A.G. (2007) Predictability of June–September rainfall in Ethiopia. Monthly Weather Review, 135, 628–650.
- Korecha, D. and Sorteberg, A. (2013) Validation of operational seasonal rainfall forecast in Ethiopia. Water Resources Research, 49, 7681–7697.
- Li, J., Xie, S.-P., Cook, E.R., Morales, M.S., Christie, D.A., Johnson, N.C., Chen, F.H., D'Arrigo, R., Fowler, A.M., Gou, X.H. and Fang, K. (2013) El Niño modulations over the past seven centuries. *Nature Climate Change*, 3, 822–826.
- Liebmann, B., Bladé, I., Funk, C., Allured, D., Quan, X., Hoerling, M., Hoell, A., Peterson, P. and Thiaw, W.M. (2017) Climatology and interannual variability of boreal spring wet season precipitation in the eastern Horn of Africa and implications for its recent decline. *Journal of Climate*, 30, 3867–3886.
- Liebmann, B., Bladé, I., Kiladis, G.N., Carvalho, L.M., Senay, G.B., Allured, D., Leroux, S. and Funk, C. (2012) Seasonality of African precipitation from 1996 to 2009. *Journal of Climate*, 25, 4304–4322.
- Liebmann, B., Hoerling, M.P., Funk, C., Bladé, I., Dole, R.M., Allured, D., Quan, X., Pegion, P. and Eischeid, J.K. (2014) Understanding recent eastern Horn of Africa rainfall variability and change. *Journal of Climate*, 27, 8630–8645.
- Lyon, B. (2014) Seasonal drought in the greater Horn of Africa and its recent increase during the March–May long rains. *Journal of Climate*, 27, 7953–7975.
- Lyon, B., Barnston, A.G. and DeWitt, D.G. (2013) Tropical Pacific forcing of a 1998–1999 climate shift: Observational analysis and climate model results for the boreal spring season. *Climate Dynamics*, 43, 893–909.
- Lyon, B. and DeWitt, D.G. (2012) A recent and abrupt decline in the East African long rains. Geophysical Research Letters, 39, L02702. https://doi.org/10.1029/ 2011GL050337.
- Mantua, N. and Hare, S. (2002) The Pacific decadal oscillation. *Journal of Oceanography*, 58, 35–44.
- McGregor, S., Timmermann, A., England, M., Elison Timm, O. and Wittenberg, A. (2013) Inferred changes in El Niño-Southern Oscillation variance over the past six centuries. Climate of the Past. 9, 2269–2284.
- McKee, T.B., Doesken, N.J. and Kleist, J. (1993) The relationship of drought frequency and duration to time scales. In: *Proceedings of the 8th Conference on Applied Climatology, Anaheim, CA, 1993, January*, Vol. 17, No. 22. Boston, MA: American Meteorological Society, pp. 179–183.
- Michaelsen, J. (1987) Cross-validation in statistical climate forecast models. Journal of Climate and Applied Meteorology, 26, 1589–1600.
- Misra, V. (2003) The influence of Pacific SST variability on the precipitation over southern Africa. *Journal of Climate*, 16, 2408–2418.
- Neale, RB., Chen, C.-C., Gettelman, A., Lauritzen, P.H., Park, S., Williamson, D.L., Conley, A.J., Garcia, R., Kinnison, D., Lamarque, J.-F., Marsh, D., Mills, M., Smith, A.K., Tilmes, S., Vitt, F., Morrison, H., Cameron-Smith, P., Collins, W.D., Iacono, M.J., Easter, R.C., Ghan, S.J., Liu, X., Rasch, P.J. and Taylor, M.A. (2012) Description of the NCAR community atmosphere model (CAM5. 0). NCAR Technical Note NCAR/TN-486+STR, 274 pp.
- Neelin, J.D., Peters, O. and Hales, K. (2009) The transition to strong convection. Journal of the Atmospheric Sciences, 66, 2367–2384.
- Nicholson, S.E. (1997) An analysis of the ENSO signal in the tropical Atlantic and western Indian Oceans. *International Journal of Climatology*, 17, 345–375.
- Nicholson, S.E. (2015) Long-term variability of the East African 'short rains' and its links to large-scale factors. *International Journal of Climatology*, 35, 3979–3990
- Nicholson, S.E. (2016) An analysis of recent rainfall conditions in eastern Africa. International Journal of Climatology, 36, 526–532.
- Nicholson, S.E. (2017) Climate and climatic variability of rainfall over eastern Africa. Reviews of Geophysics, 55, 590–635.
- Nicholson, S.E. and Kim, J. (1997) The relationship of the El Niño-Southern Oscillation to African rainfall. *International Journal of Climatology*, 17, 117–135.
- Ogallo, L.J., Janowiak, J.E. and Halpert, M.S. (1988) Teleconnection between seasonal rainfall over East Africa and global sea surface temperature anomalies. Journal of the Meteorological Society of Japan, 66, 807–822.
- Rasmusson, E.G. and Carpenter, T.H. (1982) Variations in tropical sea surface temperature and surface wind fields associated with the Southern Oscillation/El Niño. Monthly Weather Review, 110, 354–384.
- Ratnam, J.V., Behera, S.K., Masumoto, Y. and Yamagata, T. (2014) Remote effects of El Niño and Modoki events on the austral summer precipitation of southern Africa. *Journal of Climate*, 27, 3802–3815.
- Reason, C., Allan, R., Lindesay, J. and Ansell, T. (2000) ENSO and climatic signals across the Indian Ocean basin in the global context. Part I:

- interannual composite patterns. International Journal of Climatology, 20, 1285-1327.
- Ropelewski, C.F. and Halpert, M.S. (1987) Global and regional scale precipitation patterns associated with the El Niño/Southern Oscillation. Monthly Weather Review, 115, 1606-1626.
- Rowell, D.P., Booth, B.B.B., Nicholson, S.E. and Good, P. (2015) Reconciling past and future rainfall trends over East Africa. Journal of Climate, 28, 9768-9788.
- Saji, N. and Yamagata, T. (2003) Possible impacts of Indian Ocean dipole mode events on global climate. Climate Research, 25, 151-169.
- Saji, N.H., Goswami, B.N., Vinayachandran, P.N. and Yamagata, T. (1999) A dipole mode in the tropical Indian Ocean. Nature, 401, 360-363.
- Solomon, A. and Newman, M. (2012) Reconciling disparate twentieth-century Indo-Pacific ocean temperature trends in the instrumental record. Nature Climate Change, 2, 691-699.
- Taylor, K.E., Stouffer, R.J. and Meehl, G.A. (2011) An overview of CMIP5 and the experiment design. Bulletin of the American Meteorological Society, 93,
- Tierney, J., Smerdon, J., Anchukaitis, K. and Seager, R. (2013) Multidecadal variability in East African hydroclimate controlled by the Indian Ocean. Nature, 493 389-392
- Tierney, J.E., Ummenhofer, C.C. and deMenocal, P.B. (2015) Past and future rainfall in the Horn of Africa. Science Advances, 1, 1-8.
- Ummenhofer, C.C., Gupta, A.S., England, M.H. and Reason, C.J.C. (2009) Contributions of Indian Ocean sea surface temperatures to enhanced East African rainfall. Journal of Climate, 22, 993-1013.
- Verdin, J., Funk, C., Senay, G. and Choularton, R. (2005) Climate science and famine early warning. Philosophical Transactions of the Royal Society B, 360, 2155-2168.

- Vigaud, N., Lyon, B. and Giannini, A. (2017) Sub-seasonal teleconnections between convection over the Indian Ocean, the East African long rains and tropical Pacific surface temperatures. International Journal of Climatology, 37 1167-1180
- Williams, A. and Funk, C. (2010) A westward extension of the tropical Pacific warm pool leads to March through June drying in Kenya and Ethiopia,
- Williams, P. and Funk, C. (2011) A westward extension of the warm pool leads to a westward extension of the Walker circulation, drying eastern Africa. Climate Dynamics 37 2417-2435
- Wittenberg, A.T. (2009) Are historical records sufficient to constrain ENSO simulations? Geophysical Research Letters, 36, L12702. https://doi.org/10.1029/ 2009GL038710.
- Yang, W., Seager, R., Cane, M.A. and Lyon, B. (2014) The East African long rains in observations and models. Journal of Climate, 27, 7185-7202.

How to cite this article: Funk C, Harrison L, Shukla S, Pomposi C, Galu G, Korecha D, Husak G, Magadzire T, Davenport F, Hillbruner C, Eilerts G, Zaitchik B, Verdin J. Examining the role of unusually warm Indo-Pacific sea-surface temperatures in recent African droughts. Q J R Meteorol Soc 2018;1-24. https://doi.org/10.1002/qj.3266